Aus der Klinik für Herzchirurgie, Herzzentrum Dresden Universitätsklinik
Direktor: Herr Prof. Dr. med. habil. Klaus Matschke

An Imaging Photoplethysmographic Analysis of the Effects of Internal Thoracic Artery Resection on Chest Wall Perfusion

Kontaktlose photoplethysmographische Analyse des Einflusses der Arteria thoracica interna Resektion auf die Brustwanddurchblutung

D i s s e r t a t i o n s s c h r i f t

zur Erlangung des akademischen Grades

Doktor der Medizin

Doctor medicinae (Dr. med.)

vorgelegt

der Medizinischen Fakultät Carl Gustav Carus

der Technischen Universität Dresden

von

MUDr., Imre, Kukel

aus Komárno – Slowakische Republik

Dresden 2021

1. Gutachter: Prof. Dr. Klaus Matschke

2. Gutachter: Prof. Dr.-Ing. Hagen Malberg

Tag der mündlichen Prüfung: 14.06.2022

Vorsitzender der Promotionskommission: Prof. Dr. Michael Gelinsky

gez.: ----------

Vorsitzender der Promotionskommission

TABLE OF CONTENTS

LIST OF FIGURES

LIST OF TABLES

ACRONYMS

AIC	Akaike information criterion
APG	air-displacement plethysmography
AU	arbitrary units
BL	Baseline – first measurement before surgery
CABG	coronary artery bypass grafting
CAD	coronary artery disease
95% CI	95% confidence interval
Df	degrees of freedom
ECG	electrocardiogram
GEA	gastroepiploic artery
GUI	graphical user interface
H144	the fourth measurement a hundred and forty-four hours - or six days - after surgery
H2	the second measurement two hours after surgery
H24	the third measurement twenty-four hours after surgery
ICC	intraclass correlation
id	patients' variable in R
IEA	inferior epigastric artery
IPG	impedance plethysmography
iPPG	imaging photoplethysmography (in some works also referred to as remote or camera photoplethysmography)
ita	chest side variable in R
ITA	internal thoracic artery (in older nomenclature internal mammary artery)
ITA side	the side of the chest from which the internal thoracic artery has been removed
LAD	left anterior descending coronary artery

LR	likelihood ratio
MI	myocardial infarction
Other side	the side of the chest from which the internal thoracic artery has not been removed
Param.	number of parameters of the model
PCI	percutaneous coronary intervention
PPG	photoplethysmography
prep	variable with three levels: Skeletonised surgical technique of the ITA side, Pedicled surgical technique of the ITA side and the Other side in R models
Residual	residual variance of the models
ROI	region of interest
roi	region of interest (ROI 1-3 and ROI 5-7) variable in R
SGP	Strain Gauge Plethysmography
SNR	signal to noise ratio
SPG	strain gauge plethysmography
SVG	saphenous vein graft
time	time of the measurement variable in R models

1. INTRODUCTION

1.1. Coronary Artery Bypass Grafting (CABG)

1.1.1. Historical Overview

The search for a surgical solution to angina pectoris started in 1899 when Francois Franck suggested ligating sympathetic pain pathways to relieve angina. A few decades later different groups started practicing surgical sympathectomy and although the results for pain relief were promising, the procedure failed to treat the underlying coronary artery disease (CAD) and thus mortality remained high in the follow-ups.

Before settling for the nowadays universally accepted coronary artery bypass grafting, there were several different approaches to surgically address the problem of reduced myocardial perfusion. Techniques creating pericardial adhesion were suggested in the hope of delivering blood to ischaemic areas of the myocardium through the creation of extracardiac anastomoses (Moritz et al., 1932). Mechanical (Case & Brachfeld, 1962) as well as chemical pericardial abrasion techniques using different irritants (powdered beef bone, aleuronat, talc) were tried out (Schildt et al., 1943). At the same time tissue flaps of different organs – the pectoral muscle, the great omentum, the lung or the jejunum - were tried out for collateralisation of the myocardium (Beck, 1935; Key et al., 1954; Lezius, 1938; O'Shaughnessy, 1936).

The first attempt to use the internal thoracic artery (ITA, previously known as the internal mammary artery, or IMA – a name that widely survives in clinical practice) to improve coronary perfusion was carried out by Fieschi in 1939 when he ligated the ITA in the second intercostal space to increase the blood flow to the coronary circuit through smaller anastomoses. This procedure also proved to reduce angina, but later studies showed no benefit when compared to sham operations and concluded that it was no better than placebo (Cobb et al., 1959; Dimond et al., 1960). The first one to show promising results with the use of the ITA was Vineberg in 1946 (Vineberg, 1946), although the method was used on dogs and involved only the transposition of the ITA next to the left anterior descending (LAD) coronary artery without surgically creating an anastomosis during the procedure. It was found that most dogs with ischaemic heart disease developed anastomoses between the transposed ITA and the LAD. This, however, had to be evaluated in light of the fact that dogs have a greater capacity to form collaterals than humans. Further experiments on dogs followed using the carotid artery as graft between the descending aorta and the coronary sinus (Beck et al., 1948), creating a direct anastomosis from the carotid artery to the coronary circulation (Murray et al., 1954). A nonsuture method of anastomosing the right ITA to the coronary circulation with a tantalum

ring was also considered (Goetz et al., 1961). It is believed that the first sutured anastomosis of the ITA to the LAD was carried out by Vasili Kolessov in 1964 in the USSR (Kolessov, 1967). In the same year, a team led by Michael DeBakey performed an aorto-coronary bypass using the saphenous vein with a continuous suture technique (Garrett et al., 1996). The first one, however, to use CABG in a systemic approach and provide reproducible results was René Favaloro (Favaloro, 1968).

After its introduction to clinical practice, because of the limited possibilities of medical therapy, CABG quickly established itself as a potentially beneficial treatment of CAD. A symptomatic improvement of CAD due to CABG was quickly apparent, but operative mortality remained as high as 10% in some large series (Mundth & Austen, 1975a). The initially reported perioperative myocardial infarction (MI) rate of 15% (Mundth & Austen, 1975b) was raising further doubts about the benefit of CABG in reducing long-time mortality and preventing further MI. To answer this, several retrospective and prospective (randomized) studies were performed to determine the efficacy of CABG when compared to optimised medical therapy including the use of β-blockers, developed, and introduced in the meantime.

The first studies concluded that - with the exception of patients with left main disease (Oberman et al., 1976; Talano et al., 1975) - there was no significant survival benefit of CABG over optimal medical therapy (Aronow & Stemmer, 1974; Kloster et al., 1979; Mathur et al., 1975; McIntosh & Garcia, 1978). These studies, however, were heavily criticised for their selection bias, use of historical controls, the lack of comparability of the study groups and for their small sample size. As a result, clinical decision-making was instead based on three larger trials: the Veterans Administration Cooperative Study (Detre et al., 1977), the European Coronary Surgery Study (European Coronary Surgery Study Group, 1979) and the Coronary Artery Surgery Study (Killip et al., 1981). Even though these trials did not consistently show the superiority of CABG over medical therapy, they provided the basis for later meta-analyses in seven further trials that eventually reported a survival benefit with CABG at 5 and 10 years of follow-up (Yusuf et al., 1994). With these results showing not only a benefit in the symptomatic relief of angina pectoris but also in terms of prognosis, CABG became the standard for the treatment of CAD based on empirical evidence rather than on expert opinion only.

CABG provided a long-awaited solution for patients with CAD and was therefore quickly adopted. The number of procedures rose steadily in the 1970s, reaching 114 000 procedures per year in the USA alone by 1979 (Miller Jr. et al., 1981). With the introduction of percutaneous coronary intervention (PCI) in 1978 (Grüntzig, 1978) an alternative treatment strategy for symptomatic CAD was presented. As the indications for PCI were quickly

developed for acute MI (Faxon et al., 1984) and later (with the development of bare metal stents) for stable single- and multivessel disease, the number of PCIs rose exponentially. With the development of drug eluting stents and adjuvant medical therapy PCI gained even more popularity, and CABG gradually became reserved for patients with complex lesions. Nevertheless, the number of CABG procedures continued to rise, and it was not until the turn of the millennium that PCIs started to outnumber CABGs (Gerber et al., 2007; Ulrich et al., 2003). Randomized trials during the 1990s and 2000s failed to show a clear advantage of CABG over PCI (Daemen et al., 2008; Hlatky et al., 2009; The BARI Investigators, 2007), which contributed to a further decline in the number of CABGs performed in the USA, while the number of PCIs was stagnant (Epstein et al., 2011). Even though there was significant inter-country variation, a similar trend could be observed in European countries as well (Cook et al., 2007; Ghosh et al., 2004). Most recently, the results from the SYNTAX trial (Mohr et al., 2013) and ASCERT study (Weintraub et al., 2012) have contradicted earlier findings and showed an advantage for CABG, especially in more complex lesions, which may yet again shift the ratio of CABG to PCI in favour of CABG procedures.

1.1.2. Coronary Grafts

Even though the first ever CABG was performed using an ITA graft, in the early years of coronary bypass surgery, saphenous vein graft (SVG) was used in most procedures (Miller Jr. et al., 1981). It was, however, demonstrated already in 1978 that due to graft thrombosis venous grafts fail early (FitzGibbon et al., 1978). Moreover, later failure through intimal hyperplasia and atherosclerosis was also shown (Kulik et al., 2010).

Instead of venous grafting, the surgical team working with Favaloro et al. used ITA grafts ever since the introduction of the technique, and reported by the end of 1967 248 bilateral ITA graft procedures (Favaloro et al., 1968). Throughout its history, the Cleveland Clinic has provided CABG data favouring ITA grafting (Loop et al., 1986), as well as showing the superiority of bilateral ITA grafting compared to single ITA grafting (Lytle et al., 1999). The excellent patency of the ITA graft (right or left sided) triggered a search for additional arterial grafts to revascularize non-LAD myocardial territories (whilst the LAD territory remained the exclusive domain of ITA grafts). The right gastroepiploic artery (GEA), the inferior epigastric artery (IEA) and the radial artery showed the most promise. Even though good patency of the GEA and IEA grafts was demonstrated in a large retrospective study involving 290 patients (Manapat et al., 1994), because of different technical issues, the use of these grafts has never been fully integrated into clinical practice. These issues included the need for an additional laparotomy, the limited length of the graft, variation in size and the small distal diameter of the potential graft. Due to these circumstances, the radial artery has proved to be the best arterial

alternative (or addition) to the right ITA graft. It was first considered for use in 1971 (Carpentier et al., 1973), but was discarded later after high early graft occlusion rates of 30% were reported. Its revival came in the early 1990s following the surprise discovery of patent grafts 15 years after their implantation (Acar et al., 1992). Concerns regarding its susceptibility to spasm and intimal hyperplasia, however, remained (Chardigny et al., 1993; Fisk et al., 1976). With refined surgical techniques (such as the graft harvested as a pedicle), clear indication (best suited for high-grade stenoses > 90%) and additional pharmacotherapy (local dilatation as well as postoperative vasodilator therapy), 5-year patency rates of > 90% have been reported (Deb et al., 2012).

1.1.2.1. Pedicled vs. Skeletonised Grafts.

The skeletonised harvesting technique of the ITA was introduced by Keeley in 1987 (Keeley, 1987) and involves harvesting the ITA without the surrounding tissue as opposed to the pedicled harvesting technique, which dissects 1 to 2 cm of tissue around the ITA. The skeletonised approach has since been proposed as a solution to problems resulting from pedicled ITA harvesting. Its main drawback is that it requires a meticulous dissection of the ITA at the cost of 15-20 minutes of additional operating time. Also, skeletonised harvesting runs the risk of injuring the arterial graft. The potential advantages of the skeletonised over the pedicled harvesting technique include an increased blood flow in the graft, a yield of longer grafts, decreased sternal infection rates and reduced postoperative pain. A recent overview from 2015 looking at 98 papers (Fouquet et al., 2015) was able to find relevant evidence for most of these proposed advantages. In particular, the best supported papers showed that amongst patients receiving skeletonised as opposed to pedicled CABG, wound infection rate was lower (Hu & Zhao, 2011; De Paulis et al., 2005; Peterson et al., 2003; Saso et al., 2010; Sakic et al., 2013), sternal perfusion was higher (Boodhwani et al., 2006) and there was less postoperative pain (Bawany et al., 2013; Boodhwani et al., 2006; Cohen et al., 1999).

1.2. Plethysmography

Etymologically the word plethysmography is derived from the Greek “plēthysmos” (πληθυσμός, “becoming full”) and is used in medicine to denominate techniques that rely on the measurement of volume changes of an organ or the whole body. The implementation of such technique took place in 1905, when Brodie and Russell used water as a medium to measure the change in volume (Brodie & Russell, 1905). Various approaches to measure volume change have been developed since then, giving birth to different varieties of plethysmography. Of those, the following are relevant clinically: air(-displacement) plethysmography, strain gauge plethysmography, impedance plethysmography, and photoplethysmography. (Madhavan, 2005).

1.2.1. Air-Displacement Plethysmography (APG)

In air or air-displacement plethysmography the volume of an organ is measured indirectly by measuring the volume of air it displaces inside an enclosed chamber (plethysmograph) (Madhavan, 2005). Although, by using air instead of water as a medium, the additional factor of compressibility has to be taken into account, Boyle’s Law (a fixed relationship between volume and pressure applies at constant temperatures) makes that relatively easy. The first description of an air plethysmograph device (called “Das Pneumonometer”) dates back to 1882 (Pflüger, 1882). The device was used to measure the residual capacity of lungs. Later, APG became secondary to dilution techniques in the clinical diagnostic of the lungs, and it was not until 1956 that Arthur et al. presented a rapid, practical physical method for measuring lung volumes using plethysmography (DuBois et al., 1956). Further development of the technique allowed for APG to become the foremost tool in pulmonary lung volume measurement, and rightly so, as a recent study validifying APG measurement of lung volumes against volumetric CT scans shows (Tantucci et al., 2016).

Other uses of APG include the measurement of body volume and composition. While first used on infants in the early 1900s, it was not until the 1960s that the technology allowed for stable measurement, and thus none of the early APGs were developed for common, everyday use (Madhavan, 2005). Later, in the 1980s, experimental APGs were developed for these purposes, and since then, APG has become an important alternative to traditional body composition techniques (Fields et al., 2005). According to a recent summary review from 2018, however, the accuracy of APGs has not yet reached that of the four-compartment model, which serves as the gold standard in the measurement of body composition (Mazahery et al., 2018).

Further applications of APG include the detection of hemodynamic alterations in the venous system in the study of chronic venous insufficiency. Testing can be carried out using compression cuffs, thus enhancing the applicability of APG. Of note, APG measurements are not influenced by the gravitational force and therefore have been used in various space missions to quantify the effects of microgravity on vascular tone (Madhavan, 2005).

1.2.2. Strain Gauge Plethysmography (SGP)

Strain Gauge Plethysmography was introduced in 1953 by Whitney (Whitney, 1953) and refined by Brakkee and Vendrik (Brakkee & Vendrik, 1966). The strain gauge used in SGP is a mechanical transducer that changes its electrical resistance upon deformation. For clinical study purposes, the mechanical transducer consists of an elastic tube filled with mercury or an indium-gallium metal alloy conductor. By stretching the strain gauge, the diameter of the conductor decreases thus increasing its electrical resistance. After calibration, the system can be used on limbs to measure their circumference. Theoretical considerations and mathematical modelling allow the circumference to be used for the volume estimation of the limb (Whitney, 1953). Applications of SGP include measuring the venous volume of and the maximal venous outflow from the limbs (Neumann & Maessen-Visch, 1999), as well as the assessment of orthostatic fluid shifts (Thijs et al., 2007).

1.2.3. Impedance Plethysmography (IPG)

In impedance plethysmography the volume of an electrolyte fluid is measured through changes in electrical conductivity. While first mentioned in the 1930s (Atzler & Lehmann, 1932), the procedure was popularised by Nyboer in 1950 (Nyboer et al., 1950). In IPG, resistance changes are measured by applying a weak alternative current from conductive bands taped around the limb. Due to its low voltage and a 22-100 kHz alternating current, which does not interfere with systemic neuromuscular processes, the applied current remains imperceptible to the patients. Even though the translation of resistive units into volume is not trivial and can be influenced by various factors like electrolyte concentration, red blood cell velocity or haematocrit, IPG can be efficiently used for short duration volume changes (seconds to minutes) and thus may be applied to detect deep vein thrombosis. Although IPG has not found its place in chronic venous insufficiency examination, with the rise in need for wearable monitoring devices IPG has been studied for its possible application in cuffless blood monitoring (Huynh et al., 2019; Liu et al., 2017). IPGs alternative for cuffless blood pressure monitoring in wearable devices is photoplethysmography, which is discussed below.

1.2.4. Photoplethysmography (PPG)

Like the forms of plethysmography discussed above, PPG has its origins in the first half of the twentieth century. It was first described in 1937 by Hertzman (Hertzman, 1937) and has since – through the widespread application of pulse oximetry (Moyle, 1994) - become one of the most important methods for non-invasive monitoring in clinical practice. In PPG, light is applied to the tissue, and - depending on the type of probe used - the reflected or absorbed portion of the light is measured to produce a signal. Accordingly, probes used in PPG are either reflection probes (where the light source and the detector are on the same side of the tissue), or transmission probes (where the light source and detector are placed on opposite sides). Since blood is more opaque than the surrounding tissue (Stolik et al., 2000) changes in blood volume within the tissue can easily be detected by PPG. The two types of probes have their respective advantage and disadvantages. Light can only penetrate up to 5 mm of depth in tissue (Ash et al., 2017), hence the use of transmission probes is limited to body parts small enough to allow for detection (such as fingers, toes, and earlobes). On the other hand, transmission probes can also detect deep-lying arteries, allowing for measurements such as that of peripheral blood pressure (Fukushima et al., 2013). Reflective probes can only detect pulse waves in areas that contain arterio-venous anastomoses (for example in fingers, toes, earlobes, and some regions of the face), but they can allow for additional uses, such as the detection of venous filling, in particular in deep vein thrombosis (Arora et al., 1993).

As opposed to the other, previously discussed plethysmographic techniques, the PPG output has no unit of measurement. Instead, numbers are compared to their own baseline level, thus giving a change in the amplitude of the signal as result. When plotted against time, a PPG signal consists of a steady or “direct current” (DC) component and a pulsative, or “alternating current” (AC) component. The steady component is generated by the (mostly venous) vascular content of the tissue, as well as by elements of the tissue itself. The pulsative, or “alternating current” component is in turn generated by the (mostly arterial) pulsative changes of blood volume. Depending on the focus of interest, the data can be analysed to emphasise its DC or AC signal. The development of PPG is ongoing, and it has many potential applications in the field of non-invasive monitoring. Examples include devices for measuring heart rate, respiratory rate, blood pressure and cardiac output; and for assessing autonomic functions or peripheral vascular diseases.

PPG is a powerful non-invasive technique that has earned its place in everyday clinical practice as well as in experimental models analysing perfusion and vital parameters derived from it. It is, however, limited in its non-invasiveness and applicability due to its need for contact probes and a dedicated light source for its measurements. The latest branch of photoplethysmography, the imaging photoplethysmography (iPPG) attempts to address both of these limitations.

1.2.5. Imaging Photoplethysmography (iPPG)

iPPG, like PPG, uses an optical sensor to capture light intensity variations. Non-invasiveness (1) and the ability to generate a signal without a dedicated light source (2) are important advantages of the technique. Yet, before reaching its potential for (valid) data collection, possible errors stemming from these two key aspects of the method had to be addressed. The idea of PPG has been known since 1937 (Hertzman, 1937), yet the number of publications featuring iPPG has only surged in the last two decades (Figure 1 (National Library of Medicine, 2021)). There are three possible explanations for this. First, the rapid development of image processing technologies in the last two decades has made it possible to input better raw data into iPPG than before. Second, increased computational capacity allowed for the processing of raw data within a reasonable time frame as well as for the evolution of ever smaller devices to work with iPPG. Lastly, the need for portable or handheld devices fuelled the development of non-invasive technologies such as iPPG.

Historically, PPG techniques saw ambient light as noise to be eliminated (Hummler et al., 2004; Pollard, 1970; Trivedi et al., 1997), and therefore focus was on contact probes and dedicated light sources creating the field of PPG. The first works not to consider ambient light as a disturbance were published in the 2000s (Hu et al., 2008; Wieringa et al., 2005). The extraction of iPPG data by using ambient illumination was first proposed by Takano and Ohta (Takano & Ohta, 2007). This was later perfected by Verkruysse et al. (Verkruysse et al., 2008), who demonstrated not only the possibility of (non-contact) iPPG, but also of using ambient light as light source; and of detecting iPPG signals with a commercial camera.

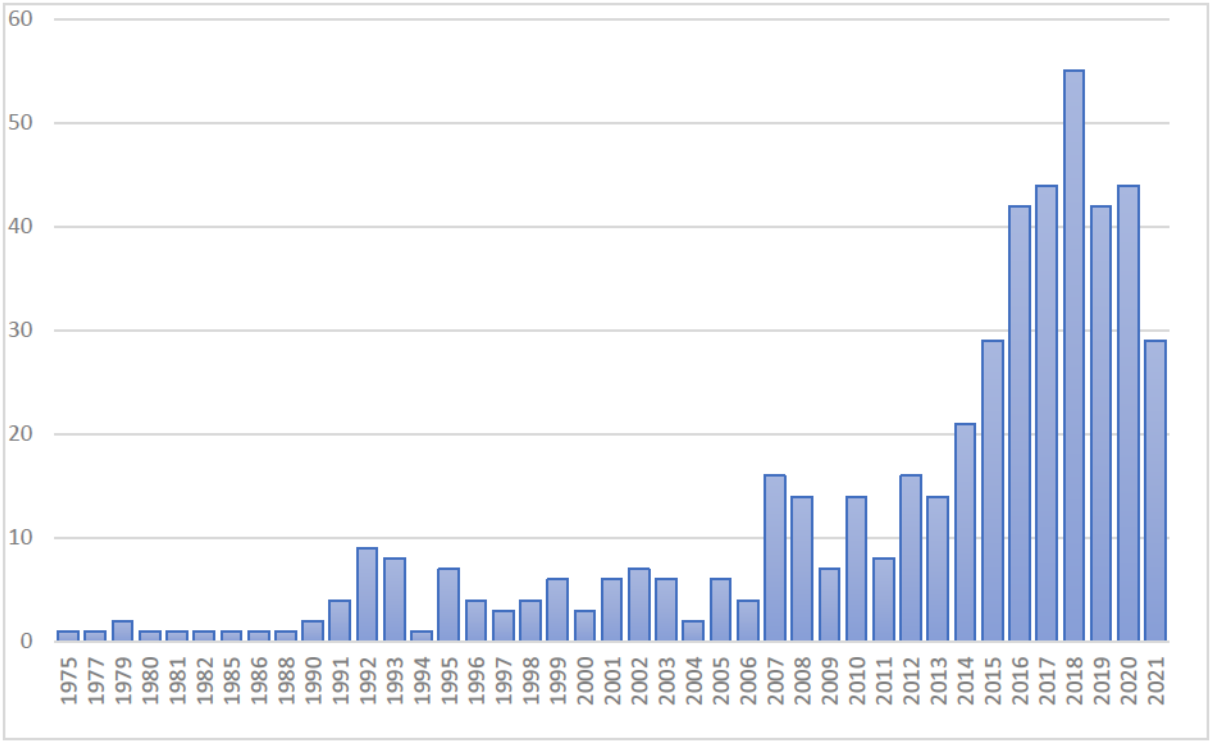

Figure 1. Number of Publications in the PubMed® Database including Imaging Photoplethysmography

According to the current state of knowledge, the iPPG signal is the result of blood volume effects and ballistocardiographic effects. Blood volume effects are caused by the variation in the amount of blood in a measured object. There are two prevailing theories to explain this variation. Based on conventional PPG theory the periodic changes in the vessels' cross-section during the heart cycle cause changes in blood volume (Weinman et al., 1977). More recently, questions arose about whether visible light (especially the green light band used in most iPPG experiments) penetrates deep enough into the tissue to reach pulsating arterioles, and therefore an alternative theory for the origin of iPPG signal was proposed by Kamshilin et al. (Kamshilin et al., 2015). According to this theory, blood volume effects are created by cyclic deformations in the dermis caused by oscillating transmural pressure changes in larger arteries. Because of the deformations, the dermis' capillary density varies, which changes the volume of blood within the measurement volume. As strong as the arguments of Kamshilin et al. might be, there are recent works that support the conventional PPG theory (Marcinkevics et al., 2016; Moço et al., 2018), as well as works showing that visible light can reach pulsating vessels and thus create an iPPG signal directly (Bashkatov et al., 2005; Reisner et al., 2008). Further research is needed to show which theory explains the origin of the iPPG signal better, or – as seems more probable at the moment – whether specific circumstances determine which theory is better suited to explain the signal origin.

The ballistocardiographic effects (or artifacts) are a pulsating component in iPPG recordings caused by body movements (Moço et al., 2016). A distinction can be made between local and global ballistocardiographic effects. Global effects are caused by distant mechanisms, such as blood ejection into the aorta causing movements of the head. Local effects are caused by local mechanisms, like for example deformations of the scanned area because of calibre changes of a larger underlying artery. As for blood volume effects, it is yet unclear to what extent ballistocardiographic effects impact iPPG signals. Studies point out that ballistocardiographic effects occur mainly in inhomogeneous and non-orthogonal illumination (when the incoming light is not perpendicular to the skin surface) (Trumpp et al., 2017), and that they are more prominent in the non-green part of the spectrum (Moço et al., 2016). It is worth noting that unlike blood volume effects (regardless of which theory explains them), which are in essence a result of the increased amount of haemoglobin in the measurement volume, ballistocardiographic effects produce a pulsating signal behaviour, which can differ substantially from the signal created through blood volume effects. Averaging values for different scanned areas – in some of which the former effect may dominate, and in other the latter – can lead to invalid results.

iPPG has been used to measure physiological data such as heart rate, heart rhythm and respiratory rate in experimental and clinical environments with high accuracy (Couderc et al., 2015; Huelsbusch & Blazek, 2002; Rasche S. et al., 2016; Tarassenko et al., 2014). As a unique feature, its signal intensity responds directly to changes in arterial blood pressure (Rasche S. et al., 2019; Trumpp et al., 2017). This haemodynamic sensitivity is linked to the peripheral vasculature of the skin, as the propagation of light into the tissue is limited to the outer skin layers. The iPPG signal is affected by autonomic nervous activity and vasomotor control in the peripheral vascular bed, like in reactions to hot and cold thermal stimuli (Trumpp et al., 2016; Volynsky et al., 2019); topically induced cutaneous vasodilation (Kamshilin et al., 2018; Marcinkevics et al., 2016); the vasodilatory effects of regional anaesthesia; and reactive hyperaemia after vascular occlusion (Marcinkevics et al., 2016). The blood volume pulse detected by iPPG is seen as an indirect measure of skin perfusion (Huelsbusch & Blazek, 2002; Rasche et al., 2020; Zheng et al., 2009). This idea has been explored in studies assessing burn wounds (Mo et al., 2015) and free flaps in plastic surgery (Secerbegovic et al., 2019), and to reveal changes in the microcirculation of the skin associated with migraine (Kamshilin et al., 2018; Zaproudina et al., 2013).

Skin perfusion is a valuable prognostic parameter, and is used to guide the therapy of critically ill patients (Hernández et al., 2019; Lima & Takala, 2014). Clinical signs of a poor skin perfusion, like mottling or a prolonged capillary refill, indicate whole body perfusion deficits during critical illness (Ait-Oufella et al., 2014; Lima et al., 2009), predict complications after major surgery (van Genderer et al., 2014), and are noted in treatment protocols for circulatory and septic shock (Dünser et al., 2013; Hernández et al., 2019). Even when perceptible signs of cutaneous malperfusion are absent, a reduction of skin perfusion is common after major surgery as a result of neurohumoral responses, an increased activity of the sympathetic nervous system and a consecutive peripheral vasoconstriction.

1.3. Hypothesis and Aim of the Thesis

Previous iPPG studies have focused on extracting vital signs from the iPPG signal, such as heart rate, respiratory rate, or oxygen saturation (McDuff et al., 2015). As described in the previous section, peripheral vasculature and the changes in its volume are key for the generation of iPPG signals. Therefore, when exploring potential applications of iPPG, one needs to consider the possibility that the iPPG signal may be associated with perfusion. The ITA is the main feeding vessel of the skin on the anterior chest wall with a restriction to the respective side of the body (Torregrossa et al., 2015). Using the ITA as a graft in CABG surgery may lead to reduced cutaneous perfusion even if collateral vascularisation of the chest wall exists as well. Previous studies (Boodhwani et al., 2006; Kamiya et al., 2008; Mamchur et al., 2020) have shown that ITA dissection can cause a disruption in sternal microcirculation, but they relied on methods other than iPPG to detect the changes (SPECT and remission spectroscopy). Recently, it was shown that, although not a direct measure, iPPG signals are strongly associated with cutaneous perfusion (Rasche et al., 2020).

The primary aim of this thesis is to answer two questions. First, is iPPG sensitive enough to detect changes corresponding to the skin perfusion alteration expected to occur after a major surgery? Second, can iPPG detect local signal changes corresponding to the skin perfusion alteration caused by the removal of the ITA from the chest circulation?

The secondary aim of this thesis is to determine whether iPPG signal differences exist between groups defined by various factors such as the colour channel of the RGB camera, or the demographic factors. Possible signal differences in groups of data from subdivisions of the chest and according to the surgical technique are also investigated.

As a special aspect of this thesis, the experimental setting consisted of a clinically feasible set-up with ambient light and a commercially available industrial-grade RGB camera. Through this set-up and by choosing a less accessible and less explored area of the body – the chest, rather than the more commonly used skin of the forehead – the robustness of the method was also tested. Moreover, it was possible to evaluate the three colour channels individually with respect to the thesis questions.

As mentioned in section 1.1.2.1, the skeletonised harvesting of the ITA is assumed to provide increased blood flow in the graft when compared to the pedicled harvesting technique. Recent studies have shown further advantages of the skeletonised harvesting technique (Fouquet et al., 2015), yet none of the studies considered the possibility that iPPG may be used to detect the difference between the two techniques. Since both surgical techniques were present in our patient collective, the signal strength was also assessed in this regard. It needs to be mentioned that, due to the nature of the study, the choice of the surgical technique was determined by external factors.

2. METHODS

2.1. Study Setting and Patients

A prospective, non-randomized observational study was designed for the Department of Cardiac Surgery, Heart Center Dresden University Hospital. The study was approved by the Institutional Review Board of the Technical University Dresden (IRB00001473, EK168052013) and was conducted in accordance with the principles of the fifth revision of the Declaration of Helsinki. Patients to be enrolled in the study were selected from the population of patients scheduled to undergo an elective coronary artery bypass surgery with the use of a unilateral ITA graft. Patients undergoing emergency surgery and patients planned for a simultaneous heart valve procedure or for a double ITA bypass were excluded from the study. There were no selection criteria regarding comorbidities, age, sex, etc. Potential candidates for the study were approached after being admitted to the hospital ward before their planned operating procedure. If an informed consent was given, the patient was enrolled in the study. All enrolled patients were informed about and allowed to leave the study at any point. Because of the nature of the study enrolment and measurements were conducted simultaneously from December 2016 to April 2017.

For each patient enrolled in the study, four video recordings were made in specific points in time before and after their surgery (later to be transformed into iPPG signals).The first and the last measurements were produces in an examination room chosen for this purpose. The second and third measurements were taken in the intensive care unit or the surgical ward at the bedside of the patients. A summary description of the measurements is provided in Table 1.

Nr.	Acronym	Timing	Place of Examination
1	BL or Baseline	Before the surgery	Examination room
2	H2	Two hours after the surgery	ICU or surgical ward
3	H24	One day or 24 hours after the surgery	ICU or surgical ward
4	H144	Six days after the surgery	Examination room

Table 1. Summary description of the measurements

2.2. Camera and Technical Setup

An industrial grade CMOS camera (UI-3370CP-C- HQ, Imaging Development System GmbH, Obersulm, Germany) with Cinegon 16/1.8 lenses (Schneider Kreuznach, Bad Kreuznach, Germany) was used. The camera was mounted on a custom-made mobile setup, allowing for a flexible and seamless integration of the measuring process into the hospital's daily workflow. (Figure 2).

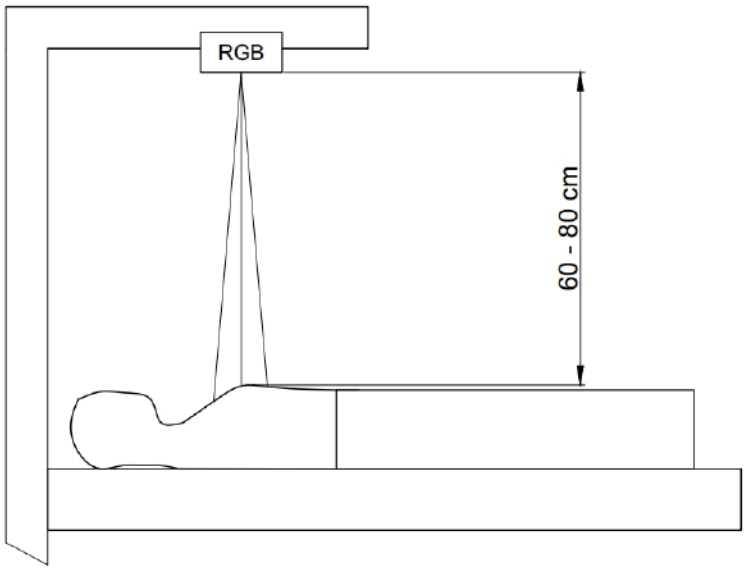

Figure 2. Schematic representation of the camera set-up

Videos were recorded with a spatial resolution of 420 x 320 pixels, a colour depth of 12 bit and a frame rate of 100 per second. Even though the equipment and the technical setup allowed for longer measurements, in order to avoid excessive patient discomfort, the duration of the measurement was initially set to 60 seconds. During the first four measurements, no patient discomfort was observed and the clinical conditions remained stable for all 60 seconds, thus the duration of the video recordings was prolonged to 180 seconds. As lack of patient discomfort and the stability of clinical conditions remained true, the rest of the measurements were conducted for 180 seconds each. Recordings were stored on a computer and analysed offline (see below).

A four-lead electrocardiogram (ECG) and a finger pulse oximetry were taken as a reference from the bedside monitor (GE Healthcare Carescape Monitor B850) at sampling rates of 300 Hz. The signals were time-synchronised with the video recordings.

No special light source was used during the measuring process. Experiments were conducted under usual ward lighting with fluorescent tubes and ambient light. The luminous colour, intensity and homogeneity of the illumination varied over the measurements, especially for measurements H2 and H24. The robustness of the models used in signal processing allows for minor variations caused by these effects, and their impact has been shown to be negligible in earlier studies (Sun et al., 2012; Verkruysse et al., 2008).

2.3. Recording Area and Regions of Interest

Former studies aiming to detect perfusion changes using iPPG have preferred the skin area on the forehead. If the only purpose of this thesis was to detect perfusion disturbances in the skin microcirculation after major surgery, a Region or Regions of Interest (ROIs) on the forehead would be the obvious choice. However, the thesis is also meant to compare the two sides of the body, one of which underwent local changes, t-o show if these changes are detectable. Hence, the choice of the chest was chosen as a target for the measurements.

Since the patients were scanned after a surgical intervention in a hospital ward, it was expected that the skin area of the chest would be partially blocked to iPPG scanning due to ECG electrodes, cables, wound drainages and dressings. It was initially unclear if these obstacles would make the scanning of the chest skin area (partially) impossible, and whether some parts of the chest would be obscured more than other. Therefore, subdivisions of the chest were defined on both sides in a symmetric fashion as additional ROIs (see below).

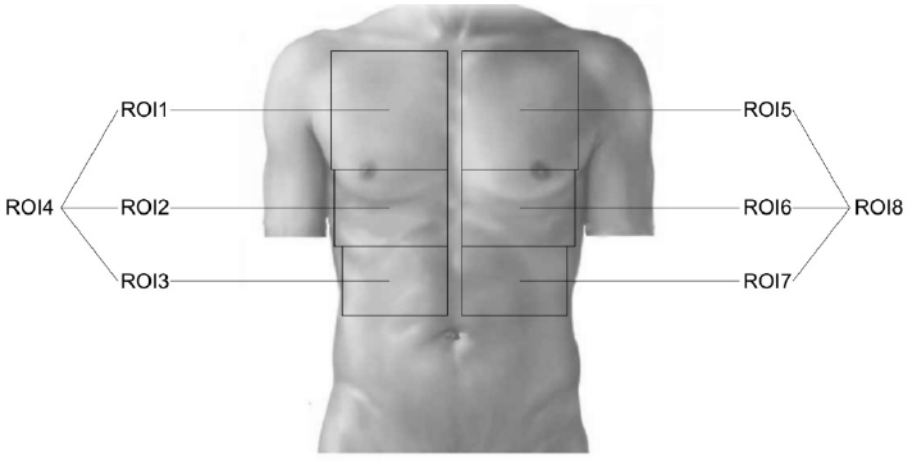

Figure 3. Selection of ROIs on the chest

For the measurement, patients assumed a supine position and the camera was positioned perpendicularly above the chest at a distance of 60 to 80 cm (Figure 2). The field of view of the camera was set to cover the entire chest wall from the clavicular line to the lower line of the ribs. The ROIs were marked manually during the offline post-processing in each individual video by a dedicated selector using the analysis software. The medial border of the ROIs was the line of the sternal bone or – if present – the edge of a postoperative patch. The lateral border was the anterior axillary line. The inferior border was the lower line of the ribs, the upper border the clavicular line. The entire area on the right side of the chest (the "ITA side") was defined as ROI 4 while the entire area on the left side ("the Other side") was defined as ROI 8. ROI 4 and ROI 8 were each subdivided into ROI 1-3 and ROI 5-7, respectively. ROI 1 and ROI 5 were defined as the area above the line of the nipples, ROI 2 and ROI 6 as the upper half of the area between the line of the nipples and the lower line of the ribcage, and ROI 3 and ROI 7 as the lower half of the area between the line of the nipples and the lower line of the ribcage (Figure 3).

2.4. Signal Processing

Signal was processed using proprietary software developed by the Institute of Biomedical Engineering of the Technical University Dresden. The details of the software algorithm and the mathematical considerations behind the signal processing go beyond the scope of this thesis, hence only a brief description will be provided here.

Data was processed within a custom software framework, which allowed for semiautomatic offline processing guided by the clinical investigator. The software was developed in Matlab (The Mathworks Inc.). The processing consisted of multiple steps, which are briefly described below. The custom GUI allowed manual definition of ROIs (as described in the previous section). The ROIs were defined in the first frame and kept constant in size and shape throughout the recording. In order to account for small movements of the thoracic region, optical flow was used during the image processing to rectify the position of predefined ROIs.

To derive iPPG signal courses, the pixels over each ROI were averaged for each of the colour channels (red, green, and blue) of the CMOS camera. To account for the slightly inhomogeneous frame rate and potentially missing frames, the iPPG signal courses were first interpolated to a sampling frequency of 100 Hz by Matlab's Piecewise Cubic Hermite Interpolating Polynomial. Afterwards the signal courses were detrended and applied a 250 tap FIR high pass filter with a cut-off frequency of 0.5 Hz in forward and backward direction.

A signal-to-noise ratio (SNR), as described by de Haan & Jeanne (de Haan & Jeanne, 2013), was used to quantify the perfusion. The SNR was calculated in the frequency domain. It relates the power around the heart rate (fHR) and its first harmonic 2* fHR (fHR ± 5 beats per minute (bpm) and 2*fHR ± 5 bpm were used) to the overall power in the frequency range between 30 and 200 bpm. The heart rate fHR was derived from the reference ECG. SNR was calculated from signal excerpts of 10s. For each subject, a representative SNR of each ROI was calculated by averaging all 10s signal excerpts of the videorecording.

2.5. Statistical Analysis

The extracted SNR data (as described in Section 2.4) was anonymised and collected into a table with the demographic data (age, weight, height, sex), and the type of heart rhythm at the time of the measurement (sinus rhythm, atrial fibrillation, pacemaker rhythm with atrial or ventricular pacing) added (Table 2). Altogether, there were 53 976 SNR values calculated, 17992 for each colour channel. On average, for each patient at a measurement point and ROI there were about 11 SNR values calculated.

Recording time	green	id	Time	ROI	Size	Weight	Sex	Age	Rhythm
2017-03-07 14:27:35:652177	5.944911752	47957	1	5	178	96	M	71	1
2017-03-07 14:27:45:645367	7.041328201	47957	1	5	178	96	M	71	1
2017-03-07 14:27:55:648519	7.017010456	47957	1	5	178	96	M	71	1
2017-03-07 14:28:05:651667	6.063580547	47957	1	5	178	96	M	71	1
2017-03-07 14:25:15:648000	3.194548134	47957	1	6	178	96	M	71	1
2017-03-07 14:25:25:651155	5.661049369	47957	1	6	178	96	M	71	1
2017-03-07 14:25:35:644353	3.942302046	47957	1	6	178	96	M	71	1
2017-03-07 14:25:45:647502	6.398994837	47957	1	6	178	96	M	71	1

Table 2. Calculated SNR values, demographic data and heart rhythm observed during the measurement (extract).

Statistical analysis was conducted using various packages of the software R (ggplot2, lme4, lmerTest, sjPlot and the default packages (R Core Team, 2019)) suitable for our purposes. In order to assess the effect of the removal of the ITA from the chest wall circulation for graft purposes, the study sample was processed in R to cohort the signal from the side of the chest from which the ITA has been removed (“ITA side”) and from the side of the chest from which the ITA has not been removed (“Other side”).

To account for any effects of age, sex, height, weight and heart rhythm on the iPPG signal, a multivariable mixed model was constructed using the lme4 package (Bates et al., 2015) and pared down on the basis of stepwise deletion. Models were compared using likelihood ratio (LR) tests, or Wilks' test, based on Wilks' theorem (Wilks, 1938), which is a classical approach to hypothesis testing and has been implemented for models' comparison in R (Winter, 2013). The significance of fixed effects was t-tested using Satterthwaite's approximations to degrees of freedom (Satterthwaite, 1941; Kuznetsova et al., 2017). The significance level was set to $p < 0.05$. SNR values are given as estimated means and 95% confidence intervals (95 CI) derived from the model.

The effects on iPPG of both the operation and the ITA harvesting were evaluated using the lme4 package of R in a mixed effects model. Fixed effects were defined based on measurement time ("time" in R) and chest side ("ita" in R). Measurement time ("time") was defined as an ordinal variable according to the surgery. Chest side was used to assess the effects of ITA harvesting. Random effects were defined by patient, and the measurement time was nested at patient level. For further explanation, see sections 3.4-3.5.

3. RESULTS

47 male and 2 female patients were examined. The age of the patients varied from 54 to 82 years; the median age was 71 years. The patients' height and weight varied from 154 to 188 cm (median 175 cm) and from 54 kg to 120 kg (median 85 kg), respectively. All patients were in sinus rhythm before surgery. Three patients (all male) were excluded after the Baseline measurement, since the surgical procedure was changed, and no unilateral ITA graft was used (in two cases, the ITA graft was bilateral and in one case, no ITA graft was involved). Data from the whole chest (ROIs 4 and 8) was expected to be more robust than data from the subdivisions of the chest (ROIs 1-3 and ROIs 5-7 respectively) and was therefore used for all calculations, with the exception of a special analysis of the data from the subdivisions of the chest, presented in in Section 3.8.

3.1. Descriptive Properties of the Data

For reasons explained in Section 2.5, the data was pre-processed to adequately represent the removal of the ITA from the supply of the chest wall (ITA side). By creating a simple model in which the only fixed variable stands for the patients, the inter-patient and the intra-patient (or patient level) variance can be determined for each colour channel (Table 3). To account for the possible influence of the individual characteristics of each patient, a random effect for patients (in R specific notation "1|id") was defined in the model (Equation 1).

$$\textbf{lmer (SNR ~ (1 | id))} \qquad \textbf{(1)}$$

Formula and data output, here as well as later on, are shown in R specific notation. For complete calculation outputs from R, see Appendix. The proportion of the patient level variance in each colour channel was calculated using Equation 2:

$$\textbf{Share of Patient Level Variance = Patient Level Variance / (Inter-Patient Variance + Patient Level Variance)} \qquad \textbf{(2)}$$

Colour channel	Inter-Patient Variance	Patient Level Variance	Proportion of Patient Level Variance	Intraclass-Correlation
Green	8.01	23.74	74.8%	22.5%
Red	2.26	13.08	85.3%	14.6%
Blue	0.97	9.37	90.6%	9.2%

Table 3. Variance and intraclass correlation of the data for the three colour channels

As presented in Table 3, patient level variance was the highest in the blue colour channel (90.6% of the whole variance), followed by the red (85.3%) and green colour channels (74.8%). Conversely, intraclass-correlation was lowest in the blue colour channel (9.2%), followed by the red colour channel (14.6%) and the green colour channel (22.5%).

3.2. Signal Strength in the Three Colour Channels

Over all measurements, signal strength was -1.80 ± 0.08 AU (Arbitrary Units; mean value ± standard error) in the green colour channel, -6.90 ± 0.06 AU in the red colour channel and -7.95 ± 0.05 AU in the blue colour channel (Table 4).

Colour Channel	Mean SNR	Standard Error	Estimate	95% CI	p
Green channel	-1.80	± 0.08	-2.22	-2.29 – -2.16	< 0.001
Red channel	-6.90	± 0,06	-6.86	-6.92 – -6.79	
Blue channel	-7.95	± 0.05	-7.87	-7.93 – -7.81	< 0.001

Table 4. Signal strength in the three colour channels over all measurements. Estimate: SNR value estimate in the simple linear model, p-Value for comparison against the red colour channel.

Due to the method of signal processing the SNR values are 10 based logarithms, meaning that the mean signal strength over all measurements was > 10^5 stronger in the green colour channel than in the red colour channel and >10^6 stronger than that in the blue colour channel. The statistical significance of the differences can be shown by using a simple linear model in R (Equation 3).

$$\text{lm (SNR ~ colour channel)} \quad (3)$$

The linear model used in Equation 3 suffices for the comparison of the SNR values of the different colour channels. An additional calculation using a linear mixed model was also done (see Equation 7 in Section 3.5 below), confirming the results (Table A4c in Appendix).

The statistical analysis built on the model from Equation 3 showed significantly different SNR values in the red and green colour channels, as well as in the red and blue colour channels ($p < 0.001$, Table 4). Since the red colour channel had the middle SNR value, it was also implied that the SNR value of the green colour channel was significantly ($p < 0.001$) stronger than that of the blue colour channel. Hence, as the large differences of the means suggested, the signal strength in the three colour channels was statistically different. Since the signal from the green colour channel was the strongest, model testing and detailed analysis of the data was based on the SNR values for the green colour channel. The data from the red and blue colour channels was used in Section 3.4 to answer one part of the hypothesis of this thesis.

3.3. Choosing a Multilevel Model

For further work with the data, the correct type of model in R had to be determined. The existence of a non-negligible intraclass-correlation (Table 3) is an argument for a multilevel (or mixed-effects) model (Mayer, 2016). Additionally, at each time of measurement, multiple SNR values were generated for the same patient (Section 2.5) and the measurements were performed over a time period rather than at the same time. Multilevel models in R are robust and can withstand possible confounders stemming from the different measurement conditions at different times of measurement (Krause & Urban, 2013; Hosoya et al., 2014).

A test of the multilevel (or mixed-effects) model was done by comparing two alternative generic models – one with and one without mixed-effects – using a likelihood ratio test (Table 5).

	Df	AIC	LR	p
Model with generalized least squares fit by maximum likelihood	2	26795		
Mixed-effects model fit by maximum likelihood	4	21945	4854	< 0.001

Table 5. Likelihood Ratio Test of the Two Models (with and without Mixed-Effects)

The generic mixed-effects model had a significantly lower AIC value ($p < 0.001$) showing that a mixed-effects (or multilevel) model was better suited to the study of the data, therefore this model structure was chosen for further analysis.

3.4. The Effect of the Major Surgery on the Signal Strength in the Three Colour Channels

After choosing a multilevel model in the previous section, it had to be adapted to convey the effect of the surgery on signal strength. We started with the basic model created in Section 3.1, in which a random effect for patients was already added (Equation 1). As stated before, the conditions – both the environment and the patients' state – were only stable during individual measurements, but not over all measurements. Hence, a variable for the time of the measurement ("time") had to be nested at the patient level into the random effect of our model (Equation 4).

$$\textbf{lmer (SNR ~ (1 | id / time)} \qquad \textbf{(4)}$$

While random effects were defined, a fixed effect of interest had to be added to the model. In order to assess the effect of the major operation on the iPPG signal over time, the time of the measurement had to be added as a fixed effect (Equation 5).

$$\textbf{lmer (SNR ~ time + (1 | id / time))} \qquad \textbf{(5)}$$

Using the model from Equation 5, all three colour channels were examined.

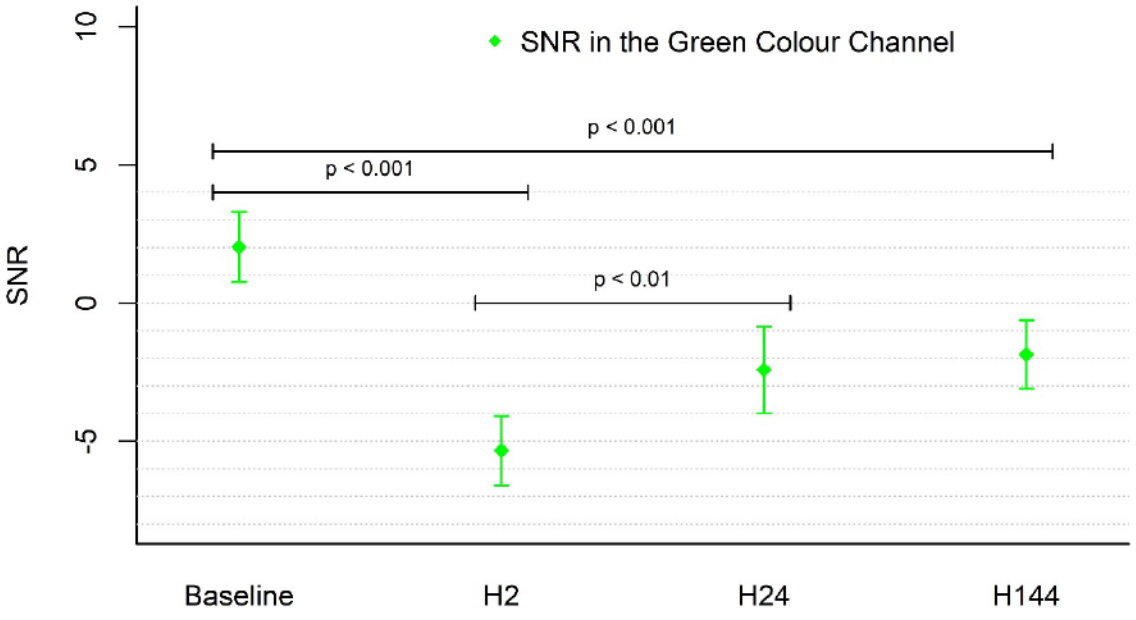

Figure 4. SNR in the Green Colour Channel over the Four Measurements. Mean estimates and 95% confidence intervals are shown.

	SNR	95% CI			p_1	Change	p_2
BL	2.02	0.75	–	3.29			
H2	-5.34	-6.59	–	-4.08	< 0.001	-7.36	< 0.001
H24	-2.42	-3.99	–	-0.85	< 0.001	2.92	< 0.01
H144	-1.86	-3.10	–	-0.63	< 0.001	0.56	0.55

Table 6. SNR in the green colour channel at the four measurement points. p_1 for comparison against the Baseline; p_2 for the change against the previous measurement point.

In the green colour channel, the Baseline signal was the strongest by a statistical margin (2.02 AU, $p_1 < 0.001$, Figure 4 and Table 6). The signal strength had a statistically significant drop from the Baseline to H2 (Δ7.36, $p_2 < 0.001$, Table 6), a (less) significant increase in strength from H2 to H24 (Δ2.92, $p_2 < 0.05$, Table 6) and a statistically not significant increase from H24 to H144 (Δ0.56, $p_2 = 0.55$). Although the signal strength increased at H144 compared to its low at H2, it has not reached the Baseline level ($p_1 < 0.001$ for difference between SNR at BL and H144, Table 6).

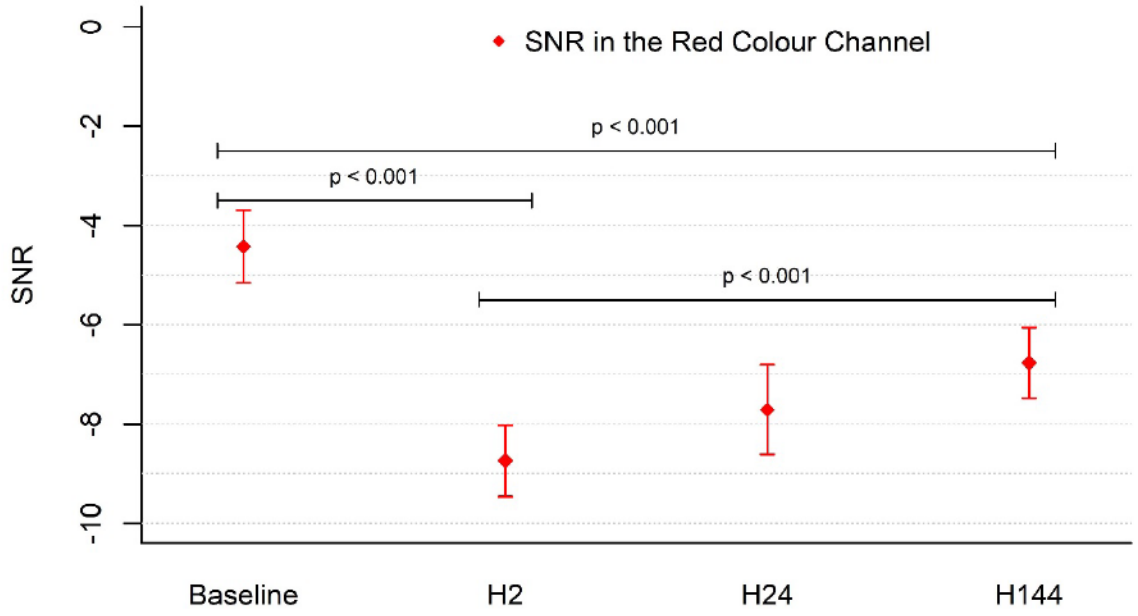

Figure 5. SNR in the Red Colour Channel over the Four Measurements. Mean estimates and 95% confidence intervals are shown.

Similarly to the data from the green colour channel, the strongest signal in the red colour channel was also observed at the Baseline ($p_1 < 0.001$ for all measurements, Figure 5 and Table 7). A statistically significant drop occurred from the Baseline to H2 ($\Delta 4.31$, $p_2 < 0.001$). The signal strength increased again from H2 to H24 and from H24 to H144, but these changes remained (albeit very slightly) under the level of statistical significance ($p_2 = 0.07$ for H2 to H24 and $p_2 = 0.09$ for H2 to H144, Table 7). Consequently, the sum of the increase from H2 to H24 and from H24 to H144 – that is, the increase from H2 to H144 – was, as expected, significant ($p < 0.001$, Table A7c in Appendix). All things considered, the signal strength in the red colour channel behaved analogously to that in the green colour channel.

	SNR	95% CI			p_1	Change	p_2
BL	-4.43	-5.16	–	-3.70			
H2	-8.74	-9.46	–	-8.02	< 0.001	-4.31	< 0.001
H24	-7.71	-8.62	–	-6.81	< 0.001	1.03	0.07
H144	-6.77	-7.48	–	-6.06	< 0.001	0.94	0.09

Table 7. SNR in the red colour channel at the four measurement points. p_1 for comparison against the Baseline; p_2 for the change against the previous measurement point.

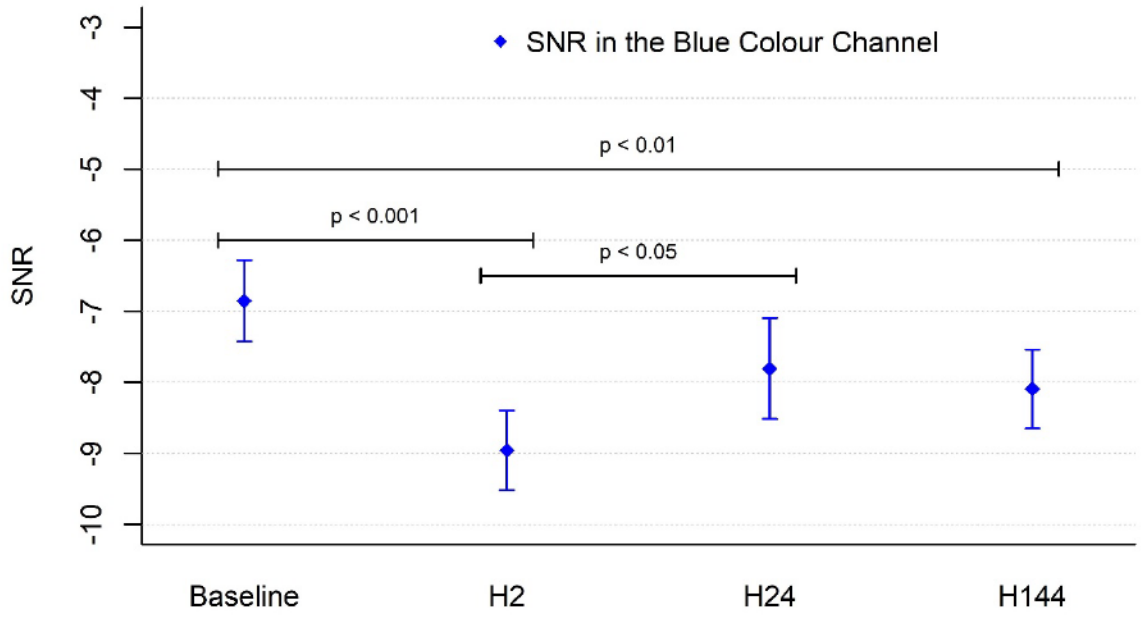

Figure 6. SNR in the Blue Colour Channel over the Four Measurements. Mean estimates and 95% confidence intervals are shown.

	SNR	95% CI			p_1	Change	p_2
BL	-6.86	-7.43	–	-6.29			
H2	-8.96	-9.52	–	-8.40	< 0.001	-2.10	< 0.001
H24	-7.81	-8.52	–	-7.10	< 0.05	1.15	< 0.05
H144	-8.09	-8.65	–	-7.54	< 0.01	-0.28	0.53

Table 8. SNR in the blue colour channel at the four measurement points. p_1 for comparison against the Baseline; p_2 for the change against the previous measurement point.

The signal in the blue colour channel was the weakest (Section 3.2) and since the signal under a certain strength level remains undetectable, the theoretical possibility to detect signal differences was the lowest for this channel. Nevertheless, the trends observed in the green and the red colour channels were also present for the blue colour. In summary: signal in the blue colour channel was strongest at the Baseline, followed by a significant drop at H2 (Δ2.10, $p_2 < 0.001$, Table 8), a significant increase from there to H24 (Δ1.15, $p_2 < 0.05$, Table 8), and then a non-significant decrease to H144 (Δ0.28, $p = 0.53$, Table 8).

3.5. The Effect of the Unilateral Resection of the Internal Thoracic Artery

The previous section looked at the global effect of major surgery on the signal strength in all three colour channels. A multilevel random effects model was defined for this purpose (Equation 5). However, with the unilateral resection of the internal thoracic artery (ITA), a unique possibility presented itself to investigate whether iPPG is sensitive enough to detect this local influence on skin perfusion. Since Equation 5 did not take into consideration the unilateral resection of the ITA, the model had to be expanded by adding a fixed effect of the chest side ("ita", Equation 6).

$$\textbf{lmer (SNR ~ time + ita + (1 | id / time))} \quad \textbf{(6)}$$

It was yet to be determined whether the addition of ita as a fixed effect was sufficient, or if it was to be set in a significant interaction with the other fixed effect, "time" (Equation 7).

$$\textbf{lmer (SNR ~ time * ita + (1 | id / time))} \quad \textbf{(7)}$$

In order to determine which model was better suited for the analysis of the data, a likelihood ratio test of the alternative models was run in R (Table 9). For comparison, previous (Equation 4 and 5) were also included.

	Residual	Param.	AIC	Chi²	Df	p
v1: green ~ (1 | id / time)	8.565	4	21945			
v2: green ~ time + (1 | id / time)	8.565	7	21894	57.205	3	< 0.001
v3: green ~ time + ita + (1 | id / time)	8.401	8	21815	81.556	1	< 0.001
v4: green ~ time * ita + (1 | id / time)	8.327	11	21781	39.453	3	< 0.001

Table 9. Likelihood ratio test of alternative models (with and without the chest side) showing the best fit and the significance of difference of the models. v1, v2, v3, v4: the respective models

The addition of "ita" alone led to a significant improvement of the model (model v3 vs. v2, AIC: 21815 < 21894, $p < 0.001$, Table 9), but coding an interaction between the two fixed effects ("ita" and "time") improved the model even further (AIC 21781 < AIC 21815, $p < 0.001$, Table 9). In other words, iPPG signal strength was affected by the chest side modulated by the time of the measurement. Therefore, the model fitted to the data was determined to be model v4 (Table 9), based on Equation 7.

Comparing the selected model with the fixed effect of the chest side (model v4, Table 9) to the model without this fixed effect (model v2, Table 9) showed that the addition of ITA harvesting as a fixed effect to the model lead to a reduction in patient level variance by 2.78% (Tables A9b and A9d in Appendix, Equation 8):

$$(8.565 - 8.327) / 8.565 = 2.78\% \quad (8)$$

Since this reduction in variance was also significant ($\sigma^2 = 8.327$ vs. $\sigma^2 = 8.565$, $\chi^2_{(df4)} = 121$, $p < 0.001$, Equation 8, Table A9f in Appendix), it can be concluded that the harvesting of the ITA significantly reduced the patient level variance and explained 2.78% of the iPPG signal variability alone.

3.6. Results from the Model Fitted to the Data

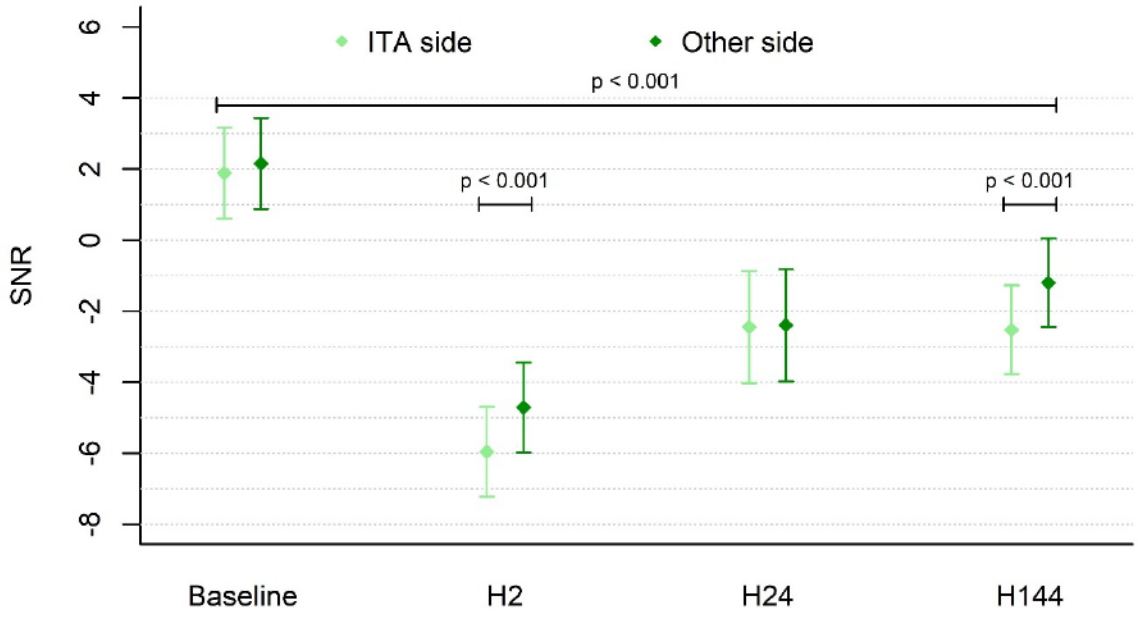

Figure 7. SNR in the Green Colour Channel by Chest Side over the Four Measurements. Mean estimates and 95% confidence intervals are shown.

SNR values estimated using our fitted model (Equation 7) were highest at the Baseline (before surgery) and dropped consistently after surgery on both sides of the chest. The lowest SNR was recorded at H2. A partial recovery of SNR occurred at H24 and H144, though SNR remained significantly below the Baseline value even at H144 (Figure 7 and Table 10).

	ITA side	95% CI		p_1	Other side	95% CI		p_2
Baseline	1.89	0.61	3.17		2.15	0.87	3.44	0.12
H2	-5.96	-7.22	-4.70	< 0.001	-4.71	-5.97	-3.45	< 0.001
H24	-2.45	-4.03	-0.87	< 0.001	-2.40	-3.98	-0.82	0.81
H144	-2.53	-3.78	-1.28	< 0.001	-1.20	-2.45	0.05	< 0.001

Table 10. SNR in the green colour channel in AU. p_1 for comparison against the Baseline; p_2 for the difference between sides.

Compared to the Baseline, SNR values at H2 decreased significantly more on the ITA side than on the Other side (Δ7.85 AU vs. Δ6.86 AU, p_3 < 0001, Table 11). Conversely, the partial recovery of SNR between H2 and H24 was higher on the ITA side (Δ3.52 AU vs. Δ2.31 AU,

$p_3 < 0.001$, Table 11). At H24, the SNR values of the two sides were comparable (-2.45 AU vs. -2.40 AU, $p_2 = 0.81$, Figure 7 and Table 10). The SNR values became significantly different at H144 (-2.53 AU for the ITA side vs. -1.20 AU for the Other side, $p_2 < 0.001$, Figure 7 and Table 10), and the overall change in SNR was significantly different between the two sides (Δ1.28 AU, $p_3 = < 0.001$, Table 11). However, the increase in SNR from H24 to H144 on the Other side was in itself not significant (Δ1.20 AU, $p_2 = 0.21$, Table 11).

	ITA side	Other side	Side difference	95% CI	p_1	p_2	p_3
BL to H2	-7.85	-6.86	0.98	0.52 – 1.45	< 0.001	< 0.001	< 0.001
H2 to H24	3.52	2.31	-1.20	-1.72 – -0.68	< 0.001	< 0.05	< 0.001
H24 to H144	-0.08	1.20	1.28	0.75 – 1.81	0.93	0.21	< 0.001

Table 11. Changes in SNR on the two sides of the chest wall, p_1 for ITA side; p_2 for the Other side; p_3 for the difference between sides.

3.7. The Effect of Cofactors

As stated in Section 2.5, the demographic data of the patients (age, weight, height, sex) as well as the type of heart rhythm at the time of the measurement were recorded. In order to analyse the effect of these factors on signal strength, they were added to the fitted multilevel model (Equation 7), creating Equation 9:

lmer (SNR ~ time * ita + (1 | id / time) + age + height + rhythm + sex + weight) **(9)**

A summary of the model (Equation 9) is shown in Table 12. As is apparent, none of these cofactors was found to have a significant impact.

Predictors	Estimates	95% CI	p
age	-0.03	-0.17 – 0.11	0.66
height	-0.05	-0.21 – 0.11	0.52
rhythm	0.03	-0.98 – 1.05	0.95
sex	-0.43	-4.99 – 4.12	0.85
weight	0.01	-0.07 – 0.08	0.88

Table 12. Effect of sex, height, weight, heart rhythm and age on signal strength. Estimates as in fitted multilevel R model.

3.8. Data from the Subdivisions of the Chest

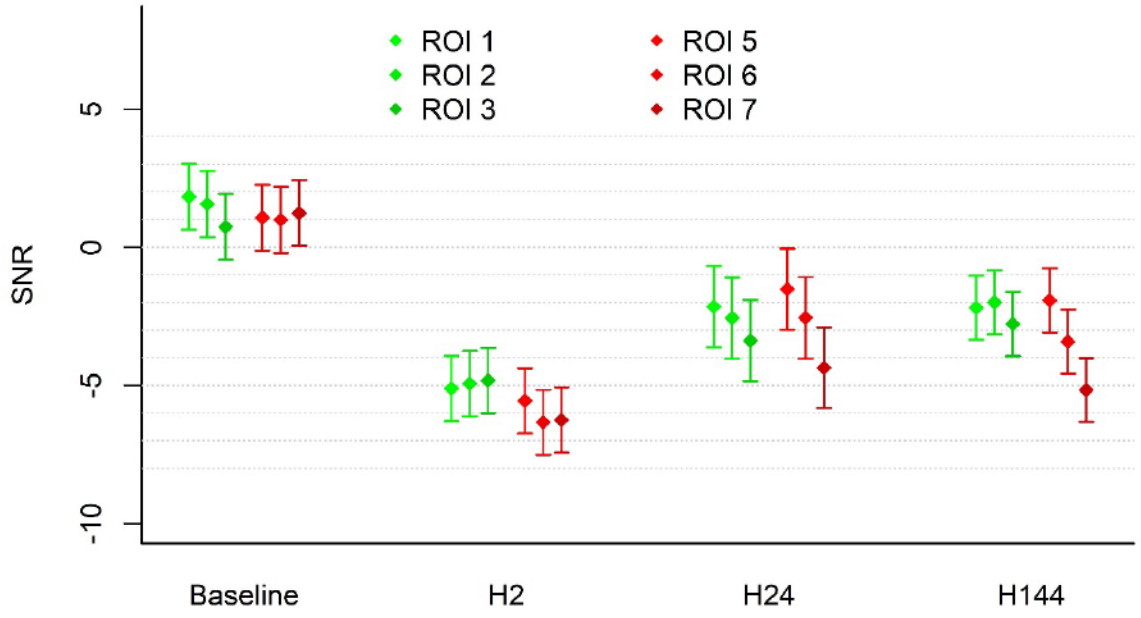

Figure 8. SNR in ROI 1 to 3 and 5 to 7. Mean estimates and 95% confidence intervals are shown.

The primary aim of this study was to analyse signal data collected from both sides of the chest, which were represented by ROIs 4 and 8 (Figure 3). However, during the recording, ROIs 1-3 and 5-7 were also defined (Section 2.3) and, accordingly, data was collected from these subdivisions of the chest. It is important to note that, by covering smaller areas, these ROIs were less robust to errors than the ones representing whole chest sides (ROI 4 and 8). Hence, comparison of individual ROIs was not undertaken; instead, the trends were assessed. In order to analyse the possible effect of location on the signal strength, the established model (Equation 7) was altered by replacing the "ita" variable with variable "roi", representing SNR values from ROIs 1-3 and 5-7 (Equation 10):

$$\textbf{lmer (SNR ~ time * roi + (1 | id / time))} \qquad \textbf{(10)}$$

Calculations based on this model (Equation 10) are shown in Figure 8 and Tables 13-14.

	ROI 1	ROI 2	ROI 3
BL	1.83 (0.62 – 3.04)	1.56 (0.35 – 2.77)	0.73 (-0.48 – 1.94)
H2	-5.11 (-6.30 – -3.92)	-4.94 (-6.13 – -3.75)	-4.82 (-6.01 – -3.63)
H24	-2.15 (-3.64 – -0.66)	-2.56 (-4.05 – -1.07)	-3.38 (-4.88 – -1.89)
H144	-2.19 (-3.37 – -1.01)	-1.99 (-3.17 – -0.81)	-2.78 (-3.96 – -1.60)

Table 13. SNR in the subdivisions of the chest on the Other side (corresponding to ROI 1-3 – Figure 3). Mean and 95% confidence intervals are shown.

	ROI 5	ROI 6	ROI 7
BL	1.07 (-0.14 – 2.28)	0.99 (-0.22 – 2.20)	1.23 (0.02 – 2.44)
H2	-5.56 (-6.75 – -4.37)	-6.34 (-7.53 – -5.15)	-6.25 (-7.45 – -5.06)
H24	-1.52 (-3.01 – -0.02)	-2.55 (-4.05 – -1.06)	-4.36 (-5.86 – -2.87)
H144	-1.92 (-3.10 – -0.74)	-3.42 (-4.60 – -2.24)	-5.17 (-6.35 – -3.99)

Table 14. SNR in the subdivisions of the chest on the ITA side (corresponding to ROI 5-7 – Figure 3). Mean and 95% confidence intervals are shown.

Similar signal strength was observed at the Baseline on both sides of the chest (ROIs 1-3 and ROIs 5-7, Figure 8). The drop in signal strength from the Baseline to H2 described in previous sections was present for all ROIs ($p < 0.001$, Figure 8 and Tables A13b/A14b in Appendix) and the increase in signal strength from H2 to H24 was also significant with one exception (ROI 3; $p < 0.001$ for ROI 5 and ROI 6; $p < 0.01$ for ROI 1, 2 and 5; $p < 0.05$ for ROI 7 and $p = 0.11$ for ROI 3). Lastly, there was no significant signal change from H24 to H144 in any of the subdivisions.

While changes over time in individual ROIs did not reveal any new trends, the signal strength at the ROIs on the ITA side showed greater variance at H24 and H144 (Figure 8 and Tables 13 and 14). Moreover, there was a ROI 7 to 5 gradient apparent at these two times of measurement, which – due to the anatomical positions of the ROIs – was effectively a caudo-cranial gradient (Figure 8). The existence of this gradient was also supported by the significant difference of the mean estimates for ROIs 5-7 at H24 and H144 in the model ($p < 0.001$ for all comparisons, Tables A13c and A13d in Appendix). A similar trend – albeit without statistical significance – could be observed on the Other side, but only at H24 (Figure 8 and Table A13e in Appendix,).

3.9. The Effect of the Surgical Technique

The choice between the skeletonised and the pedicled surgical techniques was discussed in different studies, as mentioned in Section 1.1.2.1. Since it was not the primary goal of our study to analyse the effect of the surgical technique on signal strength, there were no selection criteria for the number of cases representing the two surgical techniques. Nevertheless, by adding a variable for the surgical technique to our model, it was possible to identify any possible effects it might have had on signal strength. To accomplish this, a new variable ("prep") was created from the original variable "ita" by splitting its level "ITA side" into two: "pedicled" and "skeletonised". Thus, the new variable "prep" had three levels: "pedicled (surgical technique)", "skeletonised (surgical technique)" and "Other side of the chest". In order to create our adjusted model, the original variable "ita" was replaced by the new variable "prep" since having both would have been redundant. As in the case of "ita" (Section 3.5), we had to test whether an interaction between variables "time" and "prep" needed to be coded in the model (Equation 11) or not (Equation 10). The two alternative models together with the model without the surgical technique as a fixed effect (Equation 5), were tested using a likelihood ratio test (Table 15).

$$\textbf{lmer (SNR ~ time + prep + (1 | id / time))} \qquad \textbf{(10)}$$

$$\textbf{lmer (SNR ~ time * prep + (1 | id / time))} \qquad \textbf{(11)}$$

	Param.	AIC	Chi^2	Df	p
v1: green ~ time + (1 | id/time)	7	21894			
v2: green ~ time + prep + (1 | id/time)	9	21808	89.576	2	< 0.001
v3: green ~ time * prep + (1 | id/time)	15	21766	54.531	6	< 0.001

Table 15. Likelihood ratio test of alternative models (extending to the surgical technique) showing the best fit and the significance of the difference of the models. v1, v2, v3: the respective models.

As expected, both models with the surgical technique added as a fixed effect had lower AIC values (21808 and 21766 vs. 21894, Table 15) and significantly lower levels of residual variance (σ^2 = 8.39 vs. 8.57 and σ^2 = 8.29 vs. 8.57, both $p < 0.001$, Tables 15 and A15a, A15b and A15c in Appendix) than the model without this fixed effect. Furthermore, the model with the coded interaction between the time of the measurement and the surgical technique showed a lower AIC and level of residual variance than the model without a coded interaction between these two fixed effects (AIC = 21766 vs. 21808 and σ^2 = 8.29 vs. 8.39, $p < 0.001$ Tables 15 and A15b, A15c and A15e in Appendix). Therefore, Equation 11 was adopted to analyse the effect of the surgical technique.

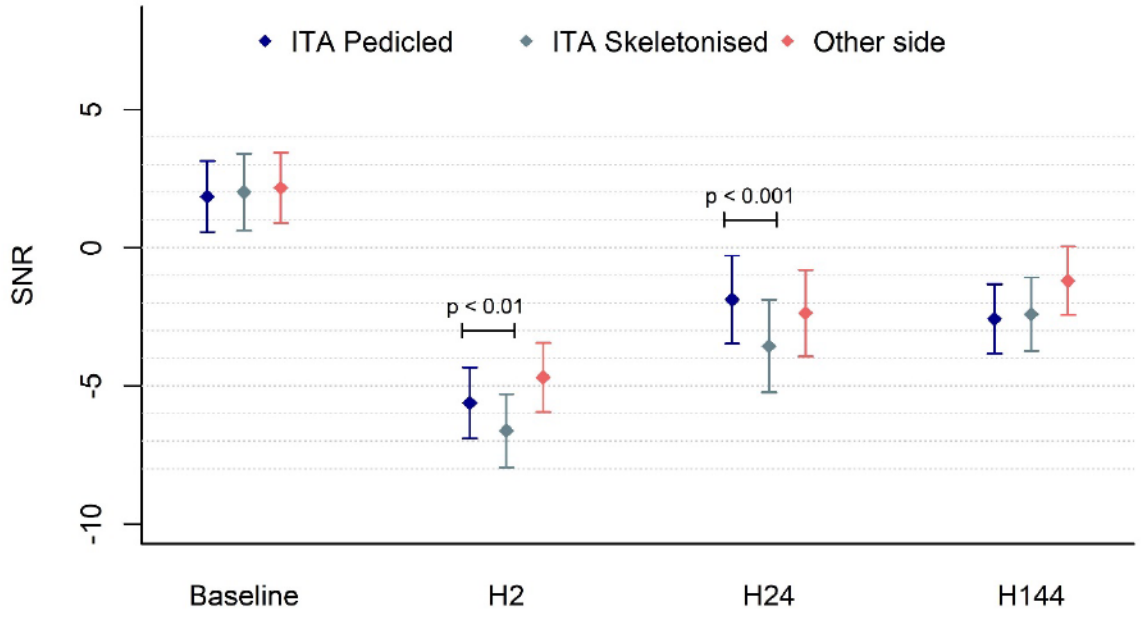

Figure 9. SNR determined by chest side and surgical technique. Mean estimates and 95% confidence intervals are shown.

Since the SNR and its changes on the Other side were analysed in previous sections, mainly data from the Pedicled and Skeletonised groups will be presented below. Data from the Other side and its comparison to the Pedicled and the Skeletonised groups will only be shown when relevant.

Figure 9 and Table 18 summarise the data from the latest model (Equation 11).

	Pedicled	Skeletonised	p_1	p_2	p_3
BL	1.85 (0.54 – 3.15)	2.01 (0.61 – 3.41)	0.12	0.65	0.67
H2	-5.62 (-6.91 – -4.33)	-6.63 (-7.97 – -5.28)	< 0.001	< 0.001	< 0.01
H24	-1.88 (-3.49 – -0.26)	-3.57 (-5.26 – -1.87)	0.053	< 0.001	< 0.001
H144	-2.58 (-3.86 – -1.31)	-2.41 (-3.76 – -1.06)	< 0.001	< 0.001	0.65

Table 16. Summary SNR values in subgroups determined by the surgical technique. Mean values and 95% confidence intervals (in parentheses) are shown. p_1 for Pedicled vs. Other side; p_2 for Skeletonised vs. Other side; p_3 for Pedicled vs. Skeletonised

At the Baseline, there was no statistical difference in SNR values between the two surgical techniques or between the surgical techniques and the Other side (p_1 = 0.12, p_2 = 0.65, p_3 = 0.67, Figure 9 and Table 16). At H2, signal strength was the strongest on the Other side, and the Pedicled surgical technique group had a stronger signal strength than the Skeletonised group (-4.71 AU vs. -5.62 AU vs. -6.63 AU, $p_1 < 0.001$ for Pedicled vs. Other side and Skeletonised vs. Other side, $p_3 < 0.01$ for Pedicled vs. Skeletonised, Figure 9 and Tables 10 and 16). By H24, signal strength was strongest in the Pedicled group (-1.88 AU vs. -3.57 AU in the Skeletonised group and -2.40 AU on the Other side, Tables 10 and 16), but the statistical significance was just under the set limit of 0.05 when compared to the Other side (p_1 = 0.053, Table 16). The signal in the Skeletonised group, however, was the weakest ($p_2 < 0.001$ vs. the Others side and $p_3 < 0.001$ vs. the Pedicled group, Figure 9 and Table 16). At H144 there was no significant difference in signal strength between the Pedicled and Skeletonised group (p_3 = 0.65, Figure 9 and Table 16), but in both ITA side groups the signal was weaker than on the Other side (both p_1 and $p_2 < 0.001$, Figure 9 and Table 16).

	Pedicled	Skeletonised	Δ	p_1	p_2	p_3
BL to H2	-7.47	-8.64	-1.17	< 0.001	< 0.001	< 0.05
H2 to H24	3.75	3.06	-0.69	< 0.001	< 0.01	0.22
H24 to H144	-0.70	1.15	1.86	0.47	0.26	< 0.01

Table 17. Changes in SNR in subgroups by the surgical technique. Δ: difference between the surgical techniques; p_1 for Pedicled group; p_2 for Skeletonised group; p_3 for the difference between the two groups.

When looking at the changes in signal strength over the four measurements, both groups of surgical technique showed the same trend as the ITA side in previous models (Section 3.6). There was a significant drop from the Baseline to H2 (p_1, $p_2 < 0.001$, Table 17), followed by a significant increase in signal strength from H2 to H24 ($p_1 < 0.001$, $p_2 < 0.01$, Table 17) and, finally, no significant change in signal strength from H24 to H144 (p_1 = 0.47, p_2 = 0.26, Table 17). When comparing the rates of change, the signal drop from the Baseline to H2 was significantly smaller in the Pedicled group (Δ = -1.17, $p_3 < 0.05$, Table 17) from H2 to H24 there was no significant difference between the two groups (p_3 = 0.22, Table 17), and, finally from H24 to H144, there was again a significant difference between the two groups ($p_3 < 0.01$, Table 17). The latter was expected, since the signal strength from H24 to H144 in the Pedicled group decreased (-0.70 AU, Figure 9 and Table 17), while in the Skeletonised group, it increased (1.15 AU, Figure 9 and Table 17), even though, as discussed above, neither of these changes was significant in itself.

4. DISCUSSION

4.1. Signal Strength in the Red, Green and Blue Colour Channels

Even though the green colour channel produced the strongest signal, iPPG was able to detect signal changes caused by the major operation in all three colour channels. In fact, the signal data showed similar trends in all three channels: a significant drop after the surgery was followed by a partial recovery of the signal strength. Importantly, as shown by the logarithmic scale, the signal strength in the red and blue colour channels was only a fraction of that in the green colour channel. It is therefore remarkable that the trends detected by iPPG in the green colour band were also detectable in the red and blue colour bands, showing not only the high sensitivity of the measurement method but also its reliability in the domain of very weak signal data. This idea was further supported by the fact that iPPG was able to reliably detect a signal variability of only 2.78% in the green colour band (Section 3.5).

It was shown in earlier studies that, when using a traditional RGB camera (which detects the colour bands red, green and blue), the strongest iPPG signal originates from the green colour channel (Tarassenko et al., 2014; Verkruysse et al., 2008). In line with this, our data showed that the green colour channel gave the strongest signal when compared to the red and blue colour channels. Possible reasons for this could be: the difference in the physical properties of the three bands; or the way in which iPPG signal is created. Red, green and blue light penetrate human tissue to different depths. Depending on the study, penetration depths have been found to be 2.5 – 4.5 mm for red light, 1 – 2.5 mm for green light and less than 1 mm for blue light (Ash et al., 2017; Bashkatov et al., 2005). In principle, the deeper penetration of red light should be an advantage when capturing signals. However, because of the anatomical characteristics of the human skin, deeper penetration means that red light reaches the lower horizontal capillary plexus as well as a significant number of veins and venous blood in the sub-cutis. While capillaries are very sensitive to (perioperative) vegetative impulses, veins are subject to other regulatory mechanisms as well. Therefore, signal generated from red light reaching the sub-cutis is likely to be less determined by changes of the microcirculation than the signal from green light. Blue light, on the other hand, with its lower penetration, fails to even completely reach the superficial vascular plexus of the skin (situated 1 – 1.5 mm below the skin surface (Braverman, 2000)), hence the blue colour channel is bound to produce a weaker signal than the green and the red channels. This was supported by our study, in which the blue colour channel provided the weakest signal.

The clinical importance of iPPG is underlined by the key role that microcirculation has had in different clinical scenarios. It has been suggested that macrocirculatory parameters, though clinically well accessible, do not adequately reflect the undergoing changes that ultimately lead to organ and systemic failures in the critically ill (Bezemer et al., 2012). Because of high mortality in the patients' group, most studies looking at microcirculation focused on sepsis and septic shock and proposed that the target of resuscitation should be the microcirculation (Brunauer et al., 2016). A recent review assessing the association between peripheral perfusion, microcirculation and mortality in sepsis showed that 23 out of 26 studies demonstrated a clear relationship between poor peripheral perfusion and mortality (Santos et al., 2019). It is apparent that monitoring microcirculation can be key to the next step of medical development in the treatment of critically ill patients. Hence the selective monitoring of the superficial vascular plexus of the skin through green light iPPG could be a valuable tool in the future.

A smaller, relative advantage of the green colour band – other than being the best fit for reflecting changes of the microcirculation – lies in the absorption spectrum of (oxy)haemoglobin, in which the green colour band exhibits the highest absorption peak, making it ideal for detecting blood in the vessels (Zijlstra & Buursma, 1997). When considering the whole optical spectrum, an absorption peak (of deoxyhaemoglobin) can also be seen at the orange and cyan bands of the spectrum. In recent studies, McDuff et al. experimented with cameras using five colour bands – with the orange and cyan bands added to the red, green and blue ones – and found that the combined data from the orange, green and cyan colour channels offered superior results than data from the green colour channel alone (McDuff et al., 2014). This advantage was not observed for other colour combinations: notably, the combined signal of the red, green and blue bands did not offer any improvement compared to the green colour band alone. While the above-mentioned physical and physiological properties explain the superiority of the green colour band compared to the red and blue ones, it is yet to be determined how addition of the signal from the orange and cyan colour band help to improve its quality.

As described in Section 1.2.5, part of the iPPG signal originates from ballistocardiographic effects – or artifacts – which are to be minimised when attempting to extract a signal from the skin microvasculature proper (Moço et al., 2016). Ballistocardiographic artifacts are stronger in the non-green spectrum of the light (Moço et al., 2016). and under non-orthogonal conditions (Trumpp et al., 2017). The former finding has led to studies using data only from the green channel or applying monochromatic cameras with green colour filters (Kamshilin et al., 2011; Sidorov et al., 2016; Zaproudina et al., 2013). Orthogonal conditions can be achieved by setting the direction of the light source as well as the direction of the recording.

As outlined in Section 2.2, the direction of the recording was orthogonal, or as close to it as clinical conditions allowed. However, since – due to the study design – no specific light source was used, the direction of the light source was non-orthogonal. Even though signal intensity differed considerably in the three colour bands (Section 3.2), the confidence intervals of the estimates were near equal. Therefore, based on the study data alone, it is not possible to say whether, and to what extent, data from the red and blue colour channels could have been influenced by ballistocardiographic artifacts. Their possible influence was, however, minimalised by basing most of the detailed analysis on the data from the green colour channel.

4.2. Signal from the Entire Chest Area

Signal data from the contact-free photoplethysmograms collected by iPPG on the chest wall of patients before and after CABG show an overall decrease in strength after the surgery, followed by a gradual but incomplete recovery until H144. They also indicate a specific impact of the unilateral ITA harvesting on the perfusion of the chest wall, which is illustrated by a steeper drop and slower recovery of the signal strength on that side of the chest wall.

These results are consistent with the cardiovascular effects of major surgery on the cutaneous circulation, and the local outcome of ITA harvesting on the perfusion of the chest wall. Depending on its extent, surgery initiates a reaction of the autonomous nervous system together with a rise in circulating catecholamine levels and local vasoconstriction (Desborough, 2000). Aiming to uphold the perfusion of vital organs, the cardiovascular reaction to a surgical trauma etiologically resembles that of shock to some degree (van Genderer et al., 2014). In such conditions the peripheral circulation is the first to be limited and the last to be fully restored (Lima & Takala, 2014). Accordingly, the number of perfused small vessels in the peripheral circulation is significantly reduced after cardiac surgery, even at a greater distance from the surgical site and is not fully restored in 24 hours (De Backer et al., 2009). The local effects of ITA harvesting include a reduced sternal perfusion, which is partially balanced out by collateral vascularization, but is still evident seven days after surgery (Carrier et al., 1992).

Earlier studies were able to detect changes in sternal perfusion after CABG, but they relied on other than iPPG to detect the changes (Boodhwani et al., 2006; Kamiya et al., 2008; Mamchur et al., 2020). Even though iPPG signals are not the same as signals of the microcirculation, the hemodynamic information content of the green band of iPPG is believed to be specific for the cutaneous microcirculation. Moreover, the cutaneous blood volume pulse is seen as the key source of iPPG (Moço et al., 2018; Trumpp et al., 2017; Zaunseder et al., 2018). This is underlined by the peak signal strength of iPPG corresponding to the absorption maximum of haemoglobin in the spectral range of green light. Therefore, using commercially available equipment, we were able to show changes in iPPG signal after a CABG surgery, indicative of changes in the cutaneous microcirculation of the overlying skin of the chest.

4.3. Signal from the Subdivisions of the Chest

To our knowledge, there have been no major studies dedicated to recording iPPG from subdivisions of the chest; nor was doing so amongst the main goals of this study. Because of that, our results have a few limitations. First, the selection of ROIs was based on generic anatomic landmarks rather than on previous studies or individually adjusted known anatomic constellations. The selection of ROIs was a semi-automated process, which may have led to a less uniform choice of skin areas over the sample population. Also, by being smaller than ROIs encompassing whole chest sides, ROIs covering subdivisions of the chest were more prone to anatomical variations and inter-individual differences of the underlying vessel structure. Due to these limitations, results from the subdivisions of the chest should be treated with reservations, and only serve as an indication for possible further directions of research.

When looking at individual ROIs, the signal strength in the subdivisions of the chest followed the same trends as that in the ROIs involving the whole chest side. At the same time, in the cluster of ROIs on the ITA side of the chest, a caudo-cranial gradient of signal strength manifested itself 24 hours after the surgery, and persisted until 6 days after it. The same trend, albeit statistically non-significant, could also be observed on the Other side 24 hours after but not 6 days after the surgery (Figure 8).

Anatomical considerations suggest that the removal of the ITA from the chest circulation should affect the caudal portions of the chest to a greater extent, because the cranial parts of the chest are closer to, and thus are likely to profit from the rich vasculature and collateralisation of the neck region. This hypothesis may be tested on a larger population or in a study that aims to show the iPPG signal differences in various parts of the chest after surgery. Also, it may be tested whether the caudal areas of the chest recover their signal strength, and if so, when that happens in comparison to the cranial subdivisions.

4.4. The Influence of the Surgical Technique on Signal Strength

While some studies (Boodhwani et al., 2006; Kamiya et al., 2008; Mamchur et al., 2020; Santos Filho et al., 2009) have argued that the skeletonised harvesting technique leads to better postoperative perfusion of the chest than the pedicled technique, others have failed to provide evidence for that. This study failed to show a statistically significant difference in signal strength between the two surgical techniques by H144 (Section 3.9). Also, according to the data from the comparison of the two chest sides (Section 3.6), by H144 the signal for both groups was weaker on the ITA side than on the Other side. What stood out in our results, however, was that at the two middle measurements (H2 and H24, both conducted within twenty-four hours after the surgery) the signal from the Pedicled group was significantly stronger than the one from the Skeletonised group.

The relevance of the Pedicled group having a stronger signal at the middle measurements is uncertain. Since no additional measurements were done between the first and the sixth day after the surgery, it cannot be said when exactly between the third and fourth measurements the difference between the Pedicled and Skeletonised groups evened out. If it was closer to the third measurement (H24), then the clinical relevance of the difference is likely to be negligible. If, however, the difference was present for a longer time, one has to wonder whether the signal strength for the Skeletonised group continues to rise and eventually leads to the Skeletonised group having a stronger signal strength than the Pedicled group. In order to answer this question, measurements beyond the seven-day scope of this thesis would have had to be made.

Notwithstanding the possible trends of signal strength, stronger signal for the Pedicled group contradicts other studies looking at perfusion after pedicled vs. skeletonised surgery techniques. There could be several reasons for this. First, our findings were made in a post hoc analysis of data that was not controlled for possible selection bias. As a result, the Pedicled group had more than twice the sample size of the Skeletonised group. The choice of technique was not randomised, and therefore patients' comorbidities, condition and the operating team's preferences could have led to biased samples. Moreover, the aforementioned studies showing a significant advantage for the Skeletonised group used a different technique (SPECT, laser Doppler flowmetric and remission spectroscopy and scintigraphy) to detect perfusion. Future prospective, randomised studies involving iPPG may be designed to control the findings of this study and others that investigated perfusion differences between groups of patients undergoing skeletonised and pedicled ITA harvesting.

5. CONCLUSION

The goal of this thesis was to investigate the sensitivity of iPPG, an emerging non-invasive monitoring method, in the setting of a large surgical procedure of CABG. Our results showed that iPPG was able to detect changes accounting for as little as 2.8% of the iPPG's signal variance. Since iPPG technology, by virtue of its non-invasiveness, targets clinical practice, where most measurements allow errors bigger than 2.8%, the magnitude of the changes detected by iPPG is remarkable. Since iPPG has a specificity for the cutaneous microcirculation, and the cutaneous blood volume pulse is associated with dermal perfusion, the measurement data was correlated with expected changes of the cutaneous microcirculation. Thus, the results of this thesis showed that iPPG was able to detect global signal changes where disruptions of the cutaneous microcirculation, resulting from CABG surgery, were expected to occur. Local signal changes, corresponding to expected alterations of the cutaneous microcirculation as a result of the ITA harvesting, were also detected by iPPG.

Of note, the results were derived from relative changes of SNR signal strength over the course of this thesis. Owing to the high variability between subjects, the SNR values of iPPG measurements, as presented here, do not allow to draw conclusions about the actual amount of cutaneous perfusion. Further studies are needed to specify iPPG in its circulatory context and to clarify artefacts and confounders affecting iPPG measurement. Hence, studies aimed at correlating and calibrating iPPG signal numbers with levels of (cutaneous) microcirculation may be carried out in the future. Subsequently, cut-off values based on clinical parameters – such as days to wound healing, wound infections – may be identified. By implementing such cut-off values, patients at risk may be identified and treated individually to foster their healing after surgery.

As discussed above, due to different reasons, the analysis of the data from the subdivisions of the chest and grouped according to the employed surgical technique has to be treated with reservations. Nevertheless, one day and six days after surgery, on the ITA side of the chest, a caudo-cranial trend of signal strengthening could be observed and deserves further investigation. The data grouped according to the surgical technique showed a stronger signal for the pedicled group, but the analysis was done post hoc on a sample not controlled for possible bias, and therefore this finding, while indicative of possible directions for future research, cannot be measured to previous literature. The demographic factors had no influence on iPPG signal strength. If supported by further studies, this feature could contribute to the robustness and universal applicability of iPPG as a measurement method.

This thesis relied on normal indoor lighting only for the experimental set-up. As shown by the results, iPPG was robust enough to withstand the lack of control of this parameter, which makes it a strong candidate not only for clinical practice, but also for the increasingly popular personal health monitoring devices. However, it is necessary to point out that a considerable amount of computational capacity was needed to produce the results, and that the evaluation of the data was not fully automated. In order to create workable personal health devices with the currently available level of computational capacity, simplification of the calculations may be necessary. Alternatively, by further developing the mathematical models used in the calculations, the demand on computational capacity may be lowered or may lead to a more automated analysis of the raw data. Another possibility to lessen the burden on computational capacity would be to revert to a dedicated light source in order to reduce the influence of artefacts. However, in this thesis we made a conscious decision to use a different set-up.

6. ABSTRACT

A prospective, non-randomized observational study involving forty-nine patients undergoing coronary artery bypass surgery (CABG) with a unilateral harvesting of the internal thoracic artery (ITA) was carried out at the Department of Cardiac Surgery, Herzzentrum Dresden University hospital. Using a commercially available industrial-grade RGB camera and normal indoor lighting, the chest wall of the patients was scanned before surgery and in three follow-up measurements.

The primary aim of this thesis was to show whether iPPG is sensitive enough to detect global signal changes after a major surgery – CABG in this case – and local signal changes due to the removal of the ITA, the main supply vessel of the chest wall. As a secondary aim, the thesis looked at subgroups of data to show if differences in signal existed between the colour channels of the RGB camera, subdivisions of the thorax and the surgical technique used as well as to show if demographic factors had an impact on signal strength.

With mathematical programs developed by the Technical University Dresden, the scanned optical data was transformed into signal to noise ratios (SNR) used in imaging photoplethysmographic (iPPG) studies. The signal data was analysed in R and, based on a stepwise deletion, a multivariable mixed effects model was constructed. Adjusted versions of this model were used for the analysis of the subgroups of the data.

Analysis of the data showed a significant decrease of iPPG signal strength after the CABG surgery with a steeper decrease and an attenuated recovery on the side of the ITA harvesting. Even though the signal variations were relatively small, using the models in this thesis, the differences were reliably detected by iPPG. The analysis of the data from the subdivisions of the chest and from patients' groups determined by the surgical technique showed a caudo-cranial signal gradient on the ITA side twenty-four hours after the surgery and a stronger signal in the Pedicled group within twenty-four hours after the surgery. The latter calculations, however, were based on a possibly biased sample and should be verified using a controlled sample in prospective randomised study designs. Demographic factors showed no significant correlation with iPPG signal strength.

iPPG was able to detect relatively small signal variations that could be associated with changes of cutaneous perfusion after major surgery. Future development could lead to non-invasive monitoring devices in the clinical practice of post-surgery care.

7. ZUSAMMENFASSUNG

Eine prospektive, nicht randomisierte Studie mit neunundvierzig Patienten geplant für eine koronare Bypassoperation (CABG) mit einseitiger Präparation der Arteria thoracica interna (ITA) wurde im Herzzentrum Dresden, Universitätsklinikum durchgeführt. In einer präoperativen und in drei postoperativen Messungen wurde die Brustwand bei den untersuchten Patienten unter normaler Innenbeleuchtung mit Hilfe einer handelsüblichen, industriellen RGB Kamera untersucht.

Das primäre Ziel der Arbeit war zu zeigen, ob iPPG als Messmethode genug Sensitivität besitzt um globale Signal-Veränderungen nach einem großen Eingriff – die CABG in diesem Fall – und lokale Signaländerung nach der Abnahme der ITA, die Hauptversorgungsarterie der Brustwand, zu erkennen. Als sekundäres Ziel der Arbeit war zu eruieren, ob iPPG Signaldifferenzen zwischen den Farbkanälen der RGB Kamera, den Brustwandaufteilungen und den Arten der ITA Präparation sowie nach den demographischen Faktoren detektieren konnte.

Die gemessenen Daten wurden unter Verwendung von Eigentumsprogrammen der Technischen Universität Dresden in den, bei plethysmographischen Studien genutzten, Signal zu Geräusch Quotienten (SNR - signal to noise ratios) umgewandelt. Die gewonnenen Signaldaten wurden in R verarbeitet und durch Verwendung der Methode schrittweise Löschung wurde ein multivariables gemischte Effekte Modell erstellt. Angepasste Versionen dieses Modells wurden für die Analyse von Patientensubgruppen verwendet.

Die Datenanalyse ergab eine signifikante Abschwächung des Signals nach der CABG, wobei die Thorax-Seite mit der ITA Präparation zeigte, im Vergleich mit der anderen Thorax-Seite, eine stärkere Abnahme und eine gedämpfte Rückbildung der Signalstärke. Obwohl die detektierte Signaländerungen relativ klein waren, sie konnten durch die entwickelten Modelle mittels iPPG zuverlässig detektiert werden. Die weitere Analyse der Daten aus den Brustwandaufteilungen und von Patientensubgruppen definiert nach Präparationsart der ITA zeigte auf der ITA Seite eine caudo-craniale Zunahme der Signalstärke ab vierundzwanzig Stunden und ein stärkeres Signal in der pedikulierten Präparationsgruppe bis vierundzwanzig Stunden nach der Operation. Allerdings, diese letztere Berechnungen wurden auf einem möglicherweise unausgewogenen Muster durchgeführt und sollten dementsprechend auf kontrollierten Mustern in prospektiven randomisierten Studien verifiziert werden. Die demographischen Faktoren hatten keiner signifikanten Korrelation mit der iPPG Signalstärke.

Die iPPG war geeignet kleine Signaländerungen assoziiert mit den erwarteten Änderungen der dermalen Perfusion bei einem großen chirurgischen Eingriff zu detektieren. Weitere Entwicklung der Technologie kann die Anwendung dieses nicht-invasive Monitoringsverfahren in der klinischen postoperativen Patientenversorgung ermöglichen.

8. REFERENCES

Acar, C., Jebara, A. V., Portoghese, M., Beyssen, B., Pagny, Y. J., Grare, P., Chachques, C. J., Fabiani, N. J., Deloche, A., & Guermonprez, L. J. (1992). Revival of the radial artery for coronary artery bypass graftng. *The Annals of Thoracic Surgery, 54*(4), 652-660. https://doi.org/10.1016/0003-4975(92)91007-V

Ait-Oufella, H., Bige, N., Boelle, P., Pichereau, C., Alves, M., Berinchamp, R., Baudel, J., Galbois, A., Maury, E., & Guidet, B. (2014). Capillary refill time exploration during septic shock. *Intensive Care Medicine, 40*, 958-964. https://doi.org/10.1007/s00134-014-3326-4

Aronow, W. S., & Stemmer, E. A. (1974). Bypass graft surgery versus medical therapy of angina pectoris. *The American Journal of Cardiology, 33*(3), 415-420. https://doi.org/10.1016/0002-9149(74)90325-7

Arora, S., Lam, D., Kennedy, C., Meier, G., Gusberg, R., & Negus, D. (1993). Light reflection rheography: a simple noninvasive screening test for deep vein thrombosis. *Journal of vascular surgery, 18*(5), 767-772. https://doi.org/10.1016/0741-5214(93)90330-O

Ash, C., Dubec, M., Donne, K., & Bashford, T. (2017). Effect of wavelength and beam width on penetration in light-tissue interaction using computational methods. *Lasers in Medical Science, 32*, 1909-1918. https://doi.org/10.1007/s10103-017-2317-4

Atzler, E., & Lehmann, G. (1932). Über ein neues Verfahren zur Darstellung der Herztätigkeit (Dielektrographie). *Arbeitsphysiologie, 5*(6), 636.

Bashkatov, A., Genina, E., Kochubey, V., & Tuchin, V. (2005). Optical properties of human skin, subcutaneous and mucous tissues in the wavelength range from 400 to 2000 nm. *Journal of Physics D: Applied Physics, 38*(15), 2543-2555. https://doi.org/10.1088/0022-3727/38/15/004

Bates, D., Maechler, M., Bolker, B., & Walker, S. (2015). Fitting Linear Mixed-Effects Models Using lme4. *Journal of Statistical Software, 67*, 1-48. https://doi.org/10.18637/jss.v067.i01

Bawany, F. I., Khan, M. S., Khan, A., & Hussain, M. (2013). Skeletonization Technique in Coronary Artery Bypass Graft Surgery Reduces the Postoperative Pain Intensity and Disability Index. *Journal of Cardiac Surgery, 29*(1), 47-50. https://doi.org/10.1111/jocs.12273

Beck, C. (1935). The development of a new blood supply to the heart by operation. *Annals of Surgery, 102*, 801-813.

Beck, C., Stanton, E., Batiuchok, W., & Leiter, E. (1948). Revascularization of heart by graft of systemic artery into coronary sinus. *Journal of the american medical association, 137*(5), 436-442.

Bezemer, R., Bartels, S. A., Bakker, J., & Ince, C. (2012). Clinical review: Clinical imaging of the sublingual microcirculation in the critically ill - where do we stand? *Crtitical Care, 16*(224). https://doi.org/10.1186/cc11236

Boodhwani, M., Lam, K., Nathan, H. J., Mesana, T. G., Ruel, M., Yeng, W., Sellke, F. W., & Rubens, F. D. (2006). Skeletonized Internal Thoracic Artery Harvest Reduces Pain and Dysesthesia and Improves Sternal Perfusion After Coronary Artery Bypass Surgery. *Circulation, 114*, 766-773. https://doi.org/10.1161/CIRCULATIONAHA.106.615427

Brakkee, A., & Vendrik, A. (1966). Strain-gauge plethysmography; theoretical and practical notes on a new design. *Journal of Applied Physiology*, 701-4. https://doi.org/10.1152/jappl.1966.21.2.701

Braverman, I. M. (2000). The Cutaneous Microcirculation. *Journal of Investigative Dermatology Symposium Proceedings, 5*(1), 3-9. https://doi.org/10.1046/j.1087-0024.2000.00010.x

Brodie, T. G., & Russell, A. E. (1905). On the determination of the rate of blood flow through an organ. *J Physiol*.

Brunauer, A., Koköfer, A., Bataar, O., Gradwohl-Matis, I., Dankl, D., Bakker, J., & Dünser, M. W. (2016). Changes in peripheral perfusion relate to visceral organ perfusion in early septic shock: A pilot study. *Journal of Critical Care, 35*, 105-109. https://doi.org/10.1016/j.jcrc.2016.05.007

Carpentier, A., Guermonprez, J. L., Deloche, A., Frechette, C., & DuBost, C. (1973). The Aorta-to-Coronary Radial Artery Bypass Graft: A Technique Avoiding Pathological Changes in Grafts. *The Annals of Thoracic Surgery, 16*(2), 111-121. https://doi.org/10.1016/S0003-4975(10)65825-0

Carrier, M., Grégoire, J., Tronc, F., Cartier, R., Leclerc, Y., & Pelletier, L.-C. (1992). Effect of internal mammary artery dissection on sternal vascularization. *The Annals of Thoracic Surgery, 53*(1), 115-119. https://doi.org/10.1016/0003-4975(92)90768-Y

Case, R. B., & Brachfeld, N. (1962). Surgical therapy of coronary arterial disease with special reference to myocardial revascularisation. *The American Journal of Cardiology, 9*(3), 425-438. https://doi.org/10.1016/0002-9149(62)90160-1

Chardigny, C., Jebara, V., Acar, C., Descombes, J., Verbeuren, T., Carpentier, A., & Fabiani, J. (1993). Vasoreactivity of the radial artery. Comparison with the internal mammary and gastroepiploic arteries with implications for coronary artery surgery. *Circulation, 88*, 15-27.

Cobb, L. A., Thomas, G. I., Dillard, D. H., Merendino, A. K., & Bruce, R. A. (1959). An Evaluation of Internal-Mammary-Artery Ligation by a Double-Blind Technic. *New England Journal of Medicine, 260*(22), 1115-1118. https://doi.org/10.1056/NEJM195905282602204

Cohen, A. J., Lockman, J., Lorberboym, M., Bder, O., Cohen, N., Medalion, B., & Chachner, A. (1999). Assessment of sternal vascularity with single photon emission computed tomography after harvesting of the internal thoracic artery. *The Journal of Thoracic and Cardiovascular Surgery, 118*(3), 496 - 502. https://doi.org/10.1016/S0022-5223(99)70188-1

Cook, S., Walker, A., Hügli, O., Togni, M., & Meier, B. (2007). Percutaneous coronary interventions in Europe. *Clinical Research in Cardiology, 96*, 375. https://doi.org/10.1007/s00392-007-0513-0

Couderc, J.-P., Kyal, S., Mestha, L. K., Xu, B., Peterson, D. R., Xia, X., & Hall, B. (2015). Detection of atrial fibrillation using contactless facial video monitoring. *Heart Rhythm, 12*(1), 195-201. https://doi.org/10.1016/j.hrthm.2014.08.035

Daemen, J., Boersma, E., Flather, M., Booth, J., Stables, R., Rodriguez, A., Rodriguez-Granillo, G., Hueb, W. A., Lemos, P. A., & Serruys, P. W. (2008). Long-Term Safety and Efficacy of Percutaneous Coronary Intervention With Stenting and Coronary Artery Bypass Surgery for Multivessel Coronary Artery Disease - A Meta-Analysis With 5-Year Patient-Level Data From the ARTS, ERACI-II, MASS-II, and SoS Trials. *Circulation, 118*, 1146-1154. https://doi.org/10.1161/CIRCULATIONAHA.107.752147

De Backer, D., Dubois, M.-J., Schmartz, D., Koch, M., Ducart, A., Barvais, L., & Vincent, J.-L. (2009). Microcirculatory Alterations in Cardiac Surgery: Effects of Cardiopulmonary Bypass and Anesthesia. *The Annals of Thoracic Surgery, 88*(5), 1396-1403. https://doi.org/10.1016/j.athoracsur.2009.07.002

de Haan, G., & Jeanne, V. (2013). Robust Pulse Rate From Chrominance-Based rPPG. *IEEE Transactions on Biomedical Engineering, 60*(10), 2878 - 2886. https://doi.org/10.1109/TBME.2013.2266196

De Paulis, R., de Notaris, S., Scaffa, R., Nadrella, S., Zeitani, J., Del Guidice, C., De Peppo, A. P., Tomai, F., & Chiariello, L. (2005). The effect of bilateral internal thoracic artery harvesting on superficial and deep sternal infection: The role of skeletonization. *The Journal of Thoracic and Cardiovascular Surgery, 129*(3), 536-543. https://doi.org/10.1016/j.jtcvs.2004.07.059

Deb, S., Cohen, E. A., Singh, S. K., Une, D., Laupacis, A., Fremes, S. E., & RAPS Investigators. (2012). Radial Artery and Saphenous Vein Patency More Than 5 Years After Coronary Artery Bypass Surgery: Results From RAPS (Radial Artery Patency Study). *Juornal of the American College of Cardiology, 60*(1), 28-35. https://doi.org/10.1016/j.jacc.2012.03.037

Desborough, J. P. (2000). The stress response to trauma and surgery. *BJA: British Journal of Anaesthesia, 85*(1), 109-117. https://doi.org/10.1093/bja/85.1.109

Detre, K., Murphy, M. L., & Hultgren, H. (1977). Effect of coronary bypass surgery on longevity in high and low risk patients: report from the VA Cooperative Coronary Surgery Study. *The Lancet, 310*(8051), 1243-1245. https://doi.org/10.1016/S0140-6736(77)92659-9

Dimond, G. E., Kittle, F. C., & Crockett, J. E. (1960). Comparison of internal mammary artery ligation and sham operation for angina pectoris. *The American Journal of Cardiology*, 483-486. https://doi.org/10.1016/0002-9149(60)90105-3

DuBois, A. B., Botelho, S. Y., Bedell, N. G., Marshall, R., & Comroe jr., J. H. (1956). A rapid plethysmographic method for measuring thoracic gas volume: a comparison with nitrogen washout method for measuring functional residual capacity in normal subjects. *The Journal of Clinical Investigation, 35*(3), 322-326. https://doi.org/https://doi.org/10.1172/JCI103281

Dünser, M. W., Takala, J., Brunauer, A., & Bakker, J. (2013). Re-thinking resuscitation: leaving blood pressure cosmetics behind and moving forward to permissive hypotension and a tissue perfusion-based approach. *Ctirical Care, 17*. https://doi.org/10.1186/cc12727

Epstein, A. J., Polsky, D., Yang, F., Yang, L., & Groeneveld, P. W. (2011). Coronary Revascularization Trends in the United States. *305*(17), 1769-1776. https://doi.org/10.1001/jama.2011.551

European Coronary Surgery Study Group. (1979). Coronary-artery bypass surgery in stable angina pectoris: survival at two years. *The Lancet, 1*(8122), 889-893.

Favaloro, R. G. (1968). Saphenous vein autograft replacement of severe segmental coronary artery occlusion: operative technique. *The Annals of thoracic surgery, 5*(4), 334-339. https://doi.org/10.1016/S0003-4975(10)66351-5

Favaloro, R. G., Effler, D. B., Groves, L. K., Fergusson, D. J., & Lozada, J. S. (1968). Double Internal Mammary Artery-Myocardial Implantation. *Circulation, 37*, 549-555. https://doi.org/10.1161/01.CIR.37.4.549

Faxon, D. P., Detre, K. M., McCabe, C. H., Fisher, L., Holmes, D. R., Cowley, M. J., Bourassa, M. G., Van Raden, M., & Ryan, T. J. (1984). Role of percutaneous transluminal coronary angioplasty in the treatment of unstable angina: Report from the national heart, lung, and blood institute percutaneous transluminal coronary angioplasty and coronary artery surgery study registries. *The American Journal of Cardiology, 53*(12), 131-135. https://doi.org/10.1016/0002-9149(84)90766-5

Fields, D. A., Higgins, P. B., & Radley, D. (2005). Air-displacement plethysmography: here to stay. *Curr Opin Clin Nutr Metab Care*, 642-9. https://doi.org/10.1097/01.mco.0000171127.44525.07

Fisk, L. R., Brooks, C. H., Callaghan, J. C., & Dvorkin, J. (1976). Experience with the Radial Artery Graft for Coronary Artery Bypass. *The Annals of Thoracic Surgery, 21*(6), 513-518. https://doi.org/10.1016/S0003-4975(10)63919-7

FitzGibbon, G. M., Burton, J. R., & Leach, A. J. (1978). Coronary bypass graft fate: angiographic grading of 1400 consecutive grafts early after operation and of 1132 after one year. *Circulation, 57*, 1070-1074. https://doi.org/10.1161/01.CIR.57.6.1070

Fouquet, O., Tariel, F., Desulauze, P., & Mével, G. (2015, May). Does a skeletonized internal thoracic artery give fewer postoperative complications than a pedicled artery for patients undergoing coronary artery bypass grafting? *Interactive CardioVascular and Thoracic Surgery, 20*(5), 663-668. https://doi.org/10.1093/icvts/ivv026

Fukushima, H., Kawanaka, H., Bhuiyan, M., & Oguri, K. (2013). Cuffless blood ressure estimation using only photoplethysmography based on cardiovascular parameters. *35th Annual International Conference of the IEEE Engineering in Medicine and Biology Society (EMBC)*, (pp. 2132-2135). Osaka. https://doi.org/10.1109/EMBC.2013.6609955

Garrett, H., Dennis, E., & DeBakey, M. (1996). Aortocoronary bypass with saphenous vein graft: seven-year follow-up. *JAMA, 223*(7), 792-794. https://doi.org/10.1001/jama.1973.03220070046012

Gerber, Y., Rihal, C. S., Sundt, T. M., Killian, J. M., Weston, S. A., Therneau, T. M., & Roger, V. L. (2007). Coronary Revascularization in the Community: A Population-Based Study, 1990 to 2004. *Journal of the American College of Cardiology, 50*(13), 1223-1229. https://doi.org/10.1016/j.jacc.2007.06.022

Ghosh, P., Schistek, R., & Unger, F. (2004). Coronary Revascularization in DACH: 1991 - 2002. *The Thoracic and Cardiovascular Surgeon, 52*(6), 356-364. https://doi.org/10.1055/s-2004-821073

Goetz, R. H., Rohman, M., Haller, J. D., Dee, R., & Rosenak, S. S. (1961). Internal mammary-coronary artery anastomosis - A nonsuture method employing tantalum rings. *The Journal of Thoracic and Cardiovascular Surgery, 41*(3), 378-386. https://doi.org/10.1016/S0022-5223(20)31701-3

Grüntzig, A. (1978). Transluminal dilatation of coronary-artery stenosis. *Lancet, 1*(8058), 263. https://doi.org/10.1016/s0140-6736(78)90500-7

Hernández, G., Ospina-Tascón, G. A., Damiani, L. P., Estenssoro, E., Dubin, A., Hurtado, J., Friedman, G., Castro, R., Alegría, L., Teboul, J.-L., Cecconi, M., Ferri, G., Jibaja, M., Pairumani, R., Fernández, P., Barahona, D., Granda-Luna, V., Cavalcanti, A. B., & Bakker, J. (2019). Effect of a Resuscitation Strategy Targeting Peripheral Perfusion Status vs Serum Lactate Levels on 28-Day Mortality Among Patients With Septic ShockThe ANDROMEDA-SHOCK Randomized Clinical Trial. *JAMA, 321*(7), 654-664. https://doi.org/10.1001/jama.2019.0071

Hertzman, A. B. (1937). Photoelectric plethysmograph of the fingers and toes in man. *Proceedings of the Society for Experimental Biology and Medicine, 39*, 529-534.

Hlatky, M. A., Boothroyd, D. B., Bravata, D. M., Boersma, E., Booth, J., Brooks, M. M., Carrié, D., Clayton, T. C., Danchin, N., Flather, M., Hamm, C. W., Hueb, W. A., Kähler, J., Sheryl, K. F., King, S. B., Kosinski, A. S., Lopes, N., McDonald, K. M., Rodriguez, A., Serruys, P., . . . Pocock, S. J. (2009). Coronary artery bypass surgery compared with percutaneous coronary interventions for multivessel disease: a collaborative analysis of individual patient data from ten randomised trials. *The Lancet, 373*(9670), 1190-1197. https://doi.org/10.1016/S0140-6736(09)60552-3

Hosoya, G., Koch, T., & Eid, M. (2014). Längsschnittdaten und Mehrebenanalyse. *Kölner Zeitschrift für Soziologie und Sozialpsychologie, 66*, 189 - 218. https://doi.org/10.1007/s11577-014-0262-9

Hu, S., Zheng, J., Chouliaras, V., & Summers, R. (2008). Feasibility of imaging photoplethysmography. *International Conference on BioMedical Engineering and Informatics* (pp. 72-75). NewYork: Institute of Electrical and Electronics Engineers. https://doi.org/10.1109/BMEI.2008.365

Hu, X., & Zhao, Q. (2011). Skeletonized Internal Thoracic Artery Harvest Improves Prognosis in High-Risk Population After Coronary Artery Bypass Surgery for Good Quality Grafts. *The Annals of Thoracic Surgery, 92*(1), 48-58. https://doi.org/10.1016/j.athoracsur.2011.03.067

Huelsbusch, M., & Blazek, V. (2002). Contactless mapping of rhythmical phenomena in tissue perfusion using PPGI. *Medical Imaging 2002.* San Diego, California, United States. https://doi.org/10.1117/12.463573

Hummler, H. D., Engelmann, A., Pohlandt, F., Högel, J., & Franz, A. R. (2004). Accuracy of pulse oximetry readings in an animal model of low perfusion caused by emerging pneumonia and sepsis. *Intensive. Care.Med., 30*, 709-713. https://doi.org/10.1007/s00134-003-2116-1

Huynh, T., Jafari, R., & Chung, W.-Y. (2019). Noninvasive Cuffless Blood Pressure Estimation Using Pulse Transit Time and Impedance Plethysmography. *IEEE transactions on bio-medical engineering*, 967-976. https://doi.org/10.1109/TBME.2018.2865751

Kamiya, H., Akhyari, P., Martens, A., Karck, M., Haverich, A., & Lichtenberg, A. (2008). Sternal microcirculation after skeletonized versus pedicled harvesting of the internal thoracic artery: A randomized study. *The Journal of Thoracic and Cardiovascular Surgery, 135*(1), 32-37. https://doi.org/10.1016/j.jtcvs.2007.09.004

Kamshilin, A. A., Miridonov, S., Teplov, V., Saarenheimo, R., & Nippolainen, E. (2011). Photoplethysmographic imaging of high spatial resolution. *Biomedical Optics Express, 2*(4), 996-1006. https://doi.org/10.1364/BOE.2.000996

Kamshilin, A. A., Nippolainen, E., Sidorov, I. S., Vasilev, P. V., Erofeev, N. P., Podolian, N. P., & Romashko, R. V. (2015). A new look at the essence of the imaging photoplethysmography. *Scientific reports, 5*. https://doi.org/10.1038/srep10494

Kamshilin, A. A., Volynsky, M. A., Khayrutdinova, O., Nurkhametova, D., Babayan, L., Amelin, A. V., Mamontov, O. V., & Giniatullin, R. (2018). Novel capsaicin-induced parameters

of microcirculation in migraine patients revealed by imaging photoplethysmography. *The Journal of Headache and Pain, 19*(43). https://doi.org/10.1186/s10194-018-0872-0

Keeley, S. B. (1987). The Skeletonized Internal Mammary Artery. *The Annals of Thoracic Surgery, 44*(3), 324-325. https://doi.org/10.1016/S0003-4975(10)62088-7

Key, J., Kergin, F., Martineau, Y., & Leckey, R. (1954). A method of supplementing the coronary circulation by a jejunal pedicle graft. *The Journal of thoracic surgery, 28*(3), 320. https://doi.org/10.1016/S0096-5588(20)30989-2

Killip, T., Fisher, L., & Mock, E. (1981). The National Heart, Lung, and Blood Institute Coronary Artery Surgery Study (CASS). *Circulation, 63*(6), 69.

Kloster, F. E., Kremkau, L. E., Ritzmann, L. W., Rahimtoola, S. H., Rösch, J., & Kanarek, P. H. (1979). Coronary Bypass for Stable Angina — A Prospective Randomized Study. *The New England Journal of Medicine, 300*(4), 149-157. https://doi.org/10.1056/NEJM197901253000401

Kolessov, V. V. (1967). Mammary artery-coronary artery anastomosis as method of treatment for angina pectoris. *The Journal of Thoracic and Cardiovascular Surgery, 54*(4), 535-544. https://doi.org/10.1016/S0022-5223(19)43061-4

Krause, T., & Urban, D. (2013). *Panel analysis with multilevel models : an application-oriented introduction.* OPUS - Publication Server of the University of Stuttgart. https://doi.org/10.18419/opus-5649

Kulik, A., Le May, M. R., Voisine, P., Tardif, J.-C., DeLarochelliere, R., Naidoo, S., Wells, G. A., Mesana, T. G., & Ruel, M. (2010). Aspirin Plus Clopidogrel Versus Aspirin Alone After Coronary Artery Bypass Grafting. *Circulation, 122*, 2680-2687. https://doi.org/10.1161/CIRCULATIONAHA.110.978007

Kuznetsova, A., Brockhoff, P. B., & Christensen, R. H. (2017). lmerTest Package: Tests in Linear Mixed Effects Models. *Journal of Statistical Software, 82*, 1-26. https://doi.org/10.18637/jss.v082.i13

Lezius, A. (1938). Lezius, Albert. Die anatomischen und funktionellen Grundlagen der künstlichen Blutversorgung des Herzmuskels durch die Lunge bei Coronararterienverschluss. *Archiv für klinische Chirurgie, 191*(1), 101-139.

Lima, A., & Takala, J. (2014). Clinical significance of monitoring perfusion in non-vital organs. *Intensive Care Medicine, 40*, 1052-1054. https://doi.org/10.1007/s00134-014-3345-1

Lima, A., Jansen, T., van Bommel, J., Ince, C., & Bakker, J. (2009). The prognostic value of the subjective assessment of peripheral perfusion in critically ill patients. *Critical Care Medicine, 37*(3), 934-938. https://doi.org/10.1097/CCM.0b013e31819869db

Liu, S.-H., Cheng, D.-C., & Su, C.-H. (2017). A Cuffless Blood Pressure Measurement Based on the Impedance Plethysmography Technique. *Sensors, 17*(5), 1176. https://doi.org/10.3390/s17051176

Loop, F. D., Lytle, B. W., Cosgrove, D. M., Stewart, R. W., Goormastic, M., Williams, G. W., Golding, L. A., Gill, C. C., Taylor, P. C., Sheldon, W. C., & Proudfit, W. L. (1986). Influence of the Internal-Mammary-Artery Graft on 10-Year Survival and Other Cardiac Events. *The New England Journal of Medicine, 314*, 1-6. https://doi.org/10.1056/NEJM198601023140101

Lytle, B. W., Blackstone, E. H., Loop, F. D., Houghtaling, P. L., Arnold, J. H., Akhrass, R., McCarthy, P., & Cosgrove, D. M. (1999). Two internal thoracic artery grafts are better than one. *The Journal of Thoracic and Cardiovascular Surgery, 117*(5), 855-872. https://doi.org/10.1016/S0022-5223(99)70365-X

Madhavan, G. (2005, September). Plethysmography. *Biomedical Instrumentation & Technology, 39*(5), 367-371. https://doi.org/10.2345/0899-8205(2005)39[367:P]2.0.CO;2

Mamchur, S., Vecherskii, Y., & Chichkova, T. (2020). Influence of Internal Thoracic Artery Harvesting on Sternal Osteoblastic Activity and Perfusion. *Diagnostics, 10*(11), 921. https://doi.org/10.3390/diagnostics10110921

Manapat, A. E., McCarthy, P. M., Lytle, B. W., Taylor, P. C., Loop, F. D., Stewart, R. W., Rosenkranz, E. R., Sapp, S. K., Miller, D., & Cosgrove, D. M. (1994). Gastroepiploic and inferior epigastric arteries for coronary artery bypass: Early results and evolving applications. *Circulation, 90*(5), 144-147.

Marcinkevics, Z., Rubins, U., Zaharans, J., Miščuks, A., Urtane, E., & Ozolina-Moll, L. (2016). Imaging photoplethysmography for clinical assessment of cutaneous microcirculation at two different depths. *Journal of Biomedical Optics, 21*(3). https://doi.org/10.1117/1.JBO.21.3.035005

Mathur, V. S., Guinn, G. A., Anastassiades, L. C., Chahine, R. A., Korompai, F. L., Montero, A. C., & Luchi, R. J. (1975). Surgical Treatment for Stable Angina Pectoris — Prospective Randomized Study. *The New England Journal of Medicine, 292*(14), 709-713. https://doi.org/ 10.1056/NEJM197504032921401

Mayer, B. (2016). *Hierarchische Lineare Modelle mit R*. Retrieved from https://rstudio-pubs-static.s3.amazonaws.com/84998_fc20913e519042f0a1d22781bc34d2ea.html#random-coefficients-modell-modell-3

Mazahery, H., von Hurst, P. R., McKinlay, C. J., Cormack, B. E., & Conlon, C. E. (2018). Air displacement plethysmography (pea pod) in full-term and pre-term infants: a comprehensive review of accuracy, reproducibility, and practical challenges. *Maternal Health, Neonatology, and Perinatology, 4*(12). https://doi.org/10.1186/s40748-018-0079-z

McDuff, D. J., Estepp, J. R., Piasecki, A. M., & Blackford, E. B. (2015). A survey of remote optical photoplethysmographic imaging methods. *2015 37th Annual International Conference of the IEEE Engineering in Medicine and Biology Society (EMBC)*, (pp. 6398 - 6404). https://doi.org/10.1109/EMBC.2015.7319857

McDuff, D., Gontarek, S., & Picard, R. W. (2014). Improvements in Remote Cardiopulmonary Measurement Using a Five Band Digital Camera. *IEEE Transactions on Biomedical Engineering, 61*(10), 2593-2601. https://doi.org/10.1109/TBME.2014.2323695

McIntosh, H. D., & Garcia, J. A. (1978). The first decade of aortocoronary bypass grafting,1967-1977. A review. *Circulation, 57*, 405-431. https://doi.org/10.1161/01.CIR.57.3.405

Miller Jr., D. W., Ivey, T. D., Bailey, W. W., Johnson, D. D., & Hessel, E. A. (1981). The practice of coronary artery bypass surgery in 1980. *The Journal of Thoracic and Cardiovascular Surgery, 81*(3), 423-427. https://doi.org/10.1016/S0022-5223(19)37609-3

Mo, W., Mohan, R., Li, W., Sellke, E. W., Fan, W., DiMaio, M. J., & Thatcher, J. E. (2015). The importance of illumination in a non-contact photoplethysmography imaging system for burn wound assessment. *Photonic Therapeutics and Diagnostics XI.* San Francisco, California, United States. https://doi.org/10.1117/12.2080699

Moço, A., Stuijk, S., & de Haan, G. (2016). Ballistocardiographic Artifacts in PPG Imaging. *IEEE Transactions on Biomedical Engineering, 63*(9), 1804-1811. https://doi.org/10.1109/TBME.2015.2502398

Moço, V. A., Stuijk, S., & de Haan, G. (2018). New insights into the origin of remote PPG signals in visible light and infrared. *Scientific Reports, 8*(1), 8501. https://doi.org/10.1038/s41598-018-26068-2

Mohr, F. W., Morice, M.-C., Kappetein, P. A., Feldman, T. E., Ståhle, E., Colombo, A., Mack, M. J., Holmes, D. R., Morel, M.-a., Van Dyck, N., Houle, V. M., Dawkins, K. D., &

Serruys, P. W. (2013). Coronary artery bypass graft surgery versus percutaneous coronary intervention in patients with three-vessel disease and left main coronary disease: 5-year follow-up of the randomised, clinical SYNTAX trial. *The Lancet, 381*(9867), 629-638. https://doi.org/10.1016/S0140-6736(13)60141-5

Moritz, A., Hudson, C., & Orgain, E. (1932). Augmentation of the extracardiac anastomoses of the coronary arteries through pericardial adhesions. *Journal of Experimental Medicine, 5*, 927-931.

Moyle, J. T. (1994). *Pulse Oximetry*. BMJ Publishing Group.

Mundth, E. D., & Austen, G. W. (1975). Surgical Measures for Coronary Heart Disease — (First of Three Parts). *The New England Journal of Medicine, 293*, 13-19. https://doi.org/10.1056/NEJM197507032930104

Mundth, E. D., & Austen, G. W. (1975). Surgical Measures for Coronary Heart Disease — (Second of Three Parts). *The New England Journal of Medicine, 293*, 75-80.

Murray, G., Redmond Porcheron, J. H., & Roschlau, W. (1954). Anastomosis of a systemic artery to the coronary. *Canadian Medical Association Journal, 71*(6), 594.

National Library of Medicine. (2021, 01 06). *PubMed.gov*. Retrieved from https://pubmed.ncbi.nlm.nih.gov/?term=imaging%20photoplethysmography&timeline=expanded

Neumann, M. H., & Maessen-Visch, B. M. (1999). Plethysmography. In J. Hafner, A.-A. Ramelet, W. Schmeller, & U. Brunner, *Management of Leg Ulcers* (pp. 114-123). Basel: Karger. https://doi.org/10.1159/000060635

Nyboer, J., Kreider, M. M., & Hannapel, L. (1950). Electrical Impedance Plethysmography A Physical and Physiologic Approach to Peripheral Vascular Study. *Circulation*, 811-821. https://doi.org/10.1161/01.CIR.2.6.811

Oberman, A., Harrel, R. R., Russell JR., R. O., Kouchoukos, N. T., Holt JR., J. H., & Rackley, C. E. (1976). Surgical versus medical treatment in disease of the left main coronary artery. *The Lancet, 308*(7986), 591-594. https://doi.org/10.1016/S0140-6736(76)90664-4

O'Shaughnessy, L. (1936). An experimental method of providing collateral circulation to the heart. *British Journal of Surgery, 23*(91), 665-670. https://doi.org/10.1002/bjs.1800239122

Peterson, M. D., Borger, M. A., Rao, V., Peniston, C. M., & Feindel, C. M. (2003). Skeletonization of bilateral internal thoracic artery grafts lowers the risk of sternal infection in patients with diabetes. *The Journal of Thoracic and Cardiovascular Surgery, 126*(5), 1314-1319. https://doi.org/10.1016/S0022-5223(03)00808-0

Pflüger, E. (1882). Das Pneumonometer. *Pflüger's Arch. f. d. ges. Physiol., 29*(244).

Pollard, J. A. (1970). Cardiac arrhythmias and pulse variability. A plethysmographic study. *Anaesthesia, 25*, 63-72.

R Core Team. (2019). R: A language and Environment for Statistical Computing. Vienna, Austria: R Foundation for Statistical Computing. Retrieved from https://www.R-project.org/

Rasche, S., Huhle, R., Junghans, E., Gama de Abreu, M., Ling, Y., Trumpp, A., & Zaunseder, S. (2020). Association of remote imaging photoplethysmography and cutaneous perfusion in volunteers. *Scientific Reports, 10*. https://doi.org/10.1038/s41598-020-73531-0

Rasche, S., Trumpp, A., Schmidt, M., Plötze, K., Gätjen, F., Malberg, H., Matschke, K., Rudolf, M., Baum, F., & Zaunseder, S. (2019). Remote Photoplethysmographic Assessment of the Peripheral Circulation in Critical Care Patients Recovering From Cardiac Surgery. *Shock, 52*(2), 174-182. https://doi.org/10.1097/SHK.0000000000001249

Rasche, S., Trumpp, A., Waldow, T., Gaetjen, F., Plötze, K., Wedekind, D., Schmidt, M., Malberg, H., Matschke, K., & Zaunseder, S. (2016). Camera-based photoplethysmography in critical care patients. *Clinical Hemorheology and Microcirculation, 64*(1), 77-90. https://doi.org/10.3233/CH-162048

Reisner, A., Shaltis, P. A., McCombie, D., Asada, H. H., Warner, D. S., & Warner, M. A. (2008). Utility of the Photoplethysmogram in Circulatory Monitoring. *Anesthesiology, 108*, 950-958. https://doi.org/10.1097/ALN.0b013e31816c89e1

Sakic, A., Chevtchik, O., Kilo, J., Schistek, R., Mueller, L. C., Ulmer, H., Grimm, M., & Ruttmann, E. (2013). Simple adaptations of surgical technique to critically reduce the risk of postoperative sternal complications in patients receiving bilateral internal thoracic arteries. *Interactive CardioVascular and Thoracic Surgery, 17*(2), 378-382. https://doi.org/10.1093/icvts/ivt089

Santos Filho, E. C., Moraes Neto, F. R., Machado e Silva, R. A., & Moraes, C. R. (2009). Should the diabetics have the internal thoracic. *Brazilian Journal of Cardiovascular Surgery, 24*(2), 157-164. https://doi.org/10.1590/S0102-76382009000200011

Santos, D. M., Quintans, J. S., Quintans-Junior, L. J., Santana-Filho, V. J., Cunha, C. L., Menezes, I. A., & Santos, M. R. (2019). Association between peripheral perfusion, microcirculation and mortality in sepsis: a systematic review. *Revista Brasileira de Anestesiologia, 69*(6), 605-621. https://doi.org/doi.org/10.1016/j.bjane.2019.09.005

Saso, S., James, D., Vecht, J. A., Kidher, E., Kokotsakis, J., Malinovski, V., Rao, C., Darzi, A., Anderson, J. R., & Athanasiou, T. (2010). Effect of Skeletonization of the Internal Thoracic Artery for Coronary Revascularization on the Incidence of Sternal Wound Infection. *The Annals of Thoracic Surgery, 89*(2), 661-670. https://doi.org/10.1016/j.athoracsur.2009.08.018

Satterthwaite, E. F. (1941). Synthesis of variance. *Psychometrika, 6*, 309-316.

Schildt, P., Stanton, E., & Beck, C. (1943). Communications between the coronary arteries produced by the application of inflammatory agents to the surface of the heart. *Annals of Surgery, 118*(1), 34-45. https://doi.org/10.1097/00000658-194307000-00002

Secerbegovic, A., Mesic, H., Bergsland, J., & Balasingham, I. (2019). Contactless blood perfusion assessment of the free flap in breast reconstruction surgery. *2019 13th International Symposium on Medical Information and Communication Technology (ISMICT)*, (pp. 1-4). Oslo, Norway. https://doi.org/10.1109/ISMICT.2019.8743657

Sidorov, I. S., Volynsky, M. A., & Kamshilin, A. A. (2016). Influence of polarization filtration on the information readout from pulsating blood vessels. *Biomedical Optics Express, 7*(7), 2469-2474. https://doi.org/10.1364/BOE.7.002469

Stolik, S., Delgado, J., Pérez, A., & Anasagasti, L. (2000). Measurement of the penetration depths of red and near infrared light in human “ex vivo” tissues. *Journal of Photochemistry and Photobiology, 57*(2-3), 90-93. https://doi.org/10.1016/S1011-1344(00)00082-8

Sun, J., Azorin-Peris, V., Kalawsky, R., Hu, S., Papin, C., & Greenwald, S. E. (2012, March 23). Use of ambient light in remote photoplethysmographic systems: comparison between a high-performance camera and a low-cost webcam. *Journal of Biomedical Optics*. https://doi.org/10.1117/1.JBO.17.3.037005

Takano, C., & Ohta, Y. (2007). Heart rate measurement based on a time-lapse image. *Med. Eng. Phys., 29*, 853-857. https://doi.org/10.1016/j.medengphy.2006.09.006

Talano, J., Scanlon, P., Meadows, W., Kahn, M., Pifarre, R., & Gunnar, R. (1975). Influence of surgery on survival in 145 patients with left main coronary artery disease. *Circulation, 52*(2), 105-11.

Tantucci, C., Bottone, D., Borghesi, A., Guerini, M., Quadri, F., & Pini, L. (2016). Methods for Measuring Lung Volumes: Is There a Better One? *Respiration, 91*, 273-280. https://doi.org/10.1159/000444418

Tarassenko, L., Villarroel, M., Guazzi, A., Jorge, J., Clifton, D., & Pugh, C. (2014). Non-contact video-based vital sign monitoring using ambient light and auto-regressive models. *Physiological Measurement, 35*, 807-831. https://doi.org/10.1088/0967-3334/35/5/807

The BARI Investigators. (2007). The Final 10-Year Follow-Up Results From the BARI Randomized Trial. *Journal of the American College of Cardiology, 49*(15), 1600 - 1606. https://doi.org/10.1016/j.jacc.2006.11.048

The Mathworks Inc. (n.d.). MATLAB. Natick, Massachusetts, USA.

Thijs, D. R., Bruijnzeels, M., Kamper, A. M., van Dijk, A. D., & van Dijk, G. J. (2007). Assessment of orthostatic fluid shifts with strain gauge plethysmography. *Clinical Science, 113*(9), 369-374. https://doi.org/10.1042/CS20070060

Torregrossa, G., Sosin, M., Gerosa, G., Tuffaha, S. H., Gottlieb, L. J., Christy, M. R., & Dorafshar, A. H. (2015). Chest Wall, Thymus, and Heart Transplant: Pushing the Boundary of Solid Organ and Vascularized Composite Allotransplantation. *Vascularized Composite Allotransplantation*, 29-36. https://doi.org/10.1080/23723505.2015.1081716

Trivedi, N. S., Ghouri, A. F., Shah, N. K., Lai, E., & Barker, S. J. (1997). Effects of motion, ambient light, and hypoperfusion on pulse oximeter function. *J. Clin. Anesth., 9*, 179-183. https://doi.org/10.1016/S0952-8180(97)00039-1

Trumpp, A., Bauer, P. L., Rasche, S., Malberg, H., & Zaunseder, S. (2017). The value of polarization in camera-based photoplethysmography. *Biomedical Optics Express, 8*(6), 2822-2834. https://doi.org/10.1364/BOE.8.002822

Trumpp, A., Rasche, S., Wedekind, D., Rudolf, M., Malberg, H., Matschke, K., & Zaunseder, S. (2017). Relation between pulse pressure and the pulsation strength in camera-based photoplethysmograms. *Current Directions in Biomedical Engineering, 3*(2), 489-492. https://doi.org/10.1515/cdbme-2017-0184

Trumpp, A., Schell, J., Malberg, H., & Zaunseder, S. (2016). Vasomotor assessment by camera-based photoplethysmography. *Current Directions in Biomedical Engineering, 2*(1), 199-202. https://doi.org/10.1515/cdbme-2016-0045

Ulrich, M. R., Brock, D. M., & Ziskind, A. A. (2003). Analysis of trends in coronary artery bypass grafting and percutaneous coronary intervention rates in Washington state from 1987 to 2001. *The American Journal of Cardiology, 92*(7), 836-839. https://doi.org/10.1016/S0002-9149(03)00895-6

van Genderer, M. E., Paauwe, J., van der Valk, R. J., Lima, A., Bakker, J., & van Bommel, J. (2014). Clinical assessment of peripheral perfusion to predict postoperative complications after major abdominal surgery early: a prospective observational study in adults. *Critical Care, 18*. https://doi.org/10.1186/cc13905

Verkruysse, W., Svaasand, L. O., & Nelson, J. S. (2008). Remote plethysmographic imaging using ambient light. *Opt. Express, 16*, 1434-1445. https://doi.org/10.1364/OE.16.021434

Vineberg, A. M. (1946). Restoration of coronary circulation by anastomosis. *Canadian Medical Association Journal, 55*(2), 117.

Volynsky, M. A., Margaryants, N. B., Mamontov, O. V., & Kamshilin, A. A. (2019). Contactless Monitoring of Microcirculation Reaction on Local Temperature Changes. *Applied Sciences, 9*(22). https://doi.org/10.3390/app9224947

Weinman, J., Hayat, A., & Raviv, G. (1977). Reflection photoplethysmography of arterial-blood-volume pulses. *Medical and Biological Engineering and Computing, 15*, 22-31. https://doi.org/10.1007/BF02441571

Weintraub, W. S., Grau-Sepulveda, M. V., Weiss, J. M., O'Brien, S. M., Peterson, E. D., Kolm, P., Zhang, Z., Klein, L. W., Shaw, R. E., McKay, C., Ritzenhaler, L. L., Popma, J. J., Messenger, J. C., Shahian, D. M., Grover, F. L., Mayer, J. E., Shewan, C. M., Garratt, K. N., Moussa, I. D., Dangas, G. D., & Edwards, F. H. (2012). Comparative Effectiveness of Revascularization Strategies. *The New England Journal of Medicine, 366*, 1467-1476. https://doi.org/10.1056/NEJMoa1110717

Whitney, R. (1953). The measurement of volume changes in human limbs. *The Journal of physiology, 121*(1), 1-27. https://doi.org/10.1113/jphysiol.1953.sp004926

Wieringa, P. F., Mastik, F., & van der Steen, A. F. (2005). Contactless multiple wavelength photoplethysmographic imaging: A first step toward "SpO(2) camera" technology. *Ann. Biomed. Eng., 33*, 1034-1041. https://doi.org/10.1007/s10439-005-5763-2

Wilks, S. S. (1938). The large sample distribution of the likelihood ratio for testing composite hypotheses. *The Annals of Mathematical Statistics, 9*(1), 60 - 62.

Winter, B. (2013). Linear models and linear mixed effects models in R with linguistic applications. *ArXiv, abs/1308.5499*. Retrieved from arXiv:1308.5499

Yusuf, S., Zucker, D., Passamani, E., Peduzzi, P., Takaro, T., Fisher, L., Kennedy, J., Davis, K., Killip, T., Norris, R., Morris, C., Mathur, V., Varnauskas, E., & Chalmers, T. (1994). Effect of coronary artery bypass graft surgery on survival: overview of 10-year results from randomised trials by the Coronary Artery Bypass Graft Surgery Trialists Collaboration. *The Lancet, 344*(8922), 563-570. https://doi.org/10.1016/S0140-6736(94)91963-1

Zaproudina, N., Teplov, V., Nippolainen, E., Jukka, L. A., & Kamshilin, A. A. (2013). Asynchronicity of Facial Blood Perfusion in Migraine. *PLoS One, 8*(12), e80189. https://doi.org/10.1371/journal.pone.0080189

Zaunseder, S., Trumpp, A., Wedekind, D., & Malberg, H. (2018). Cardiovascular assessment by imaging photoplethysmography – a review. *Biomed. Eng.-Biomed. Tech., 63*(5), 617-634. https://doi.org/0.1515/bmt-2017-0119

Zheng, J., Hu, S., Echiadis, A. S., Azorin-Peris, V., Shi, P., & Chouliaras, V. (2009). A remote approach to measure blood perfusion from the human face. *Advanced Biomedical and Clinical Diagnostic Systems VII*. San Jose, California, United States. https://doi.org/10.1117/12.807354

Zijlstra, W. G., & Buursma, A. (1997). Spectrophotometry of Hemoglobin: Absorption Spectra of Bovine Oxyhemoglobin, Deoxyhemoglobin, Carboxyhemoglobin, and Methemoglobin. *Comparative Biochemistry and Physiology Part B: Biochemistry and Molecular Biology, 118*(4), 743-749. https://doi.org/10.1016/S0305-0491(97)00230-7

9. APPENDIX

Table A3a. Variance in the Data Set, Green Colour Channel

```
summary( lmer(green ~ 1|id, data))
Linear mixed model fit by REML. t-tests use Satterthwaite's method
['lmerModLmerTest']
Formula: green ~ 1 | id
   Data: data

REML criterion at convergence: 25878.3

Scaled residuals:
    Min      1Q  Median      3Q     Max
-4.7740 -0.5756  0.0771  0.6710  2.4277

Random effects:
 Groups   Name        Variance Std.Dev.
 id       (Intercept)  8.01    2.830
 Residual             23.74    4.873
Number of obs: 4284, groups:  id, 46

Fixed effects:
            Estimate Std. Error      df t value Pr(>|t|)
(Intercept)  -1.9764     0.4267 44.1565  -4.632  3.2e-05 ***
```

Table A3b. Intraclassencorrelation of the Data, Green Colour Channel

```
ICCbare(id, green, data)
[1] 0.2250045
Warning message:
In ICCbare(id, green, data) : Missing levels of 'x' have been removed
```

Table A3c. Variance in the Data Set, Red Colour Channel

```
summary(lmer(red ~ 1|id, data))
Linear mixed model fit by REML. t-tests use Satterthwaite's method
['lmerModLmerTest']
Formula: red ~ 1 | id
   Data: data

REML criterion at convergence: 23297.5

Scaled residuals:
    Min      1Q  Median      3Q     Max
-5.2093 -0.6322  0.0371  0.6683  3.0663

Random effects:
 Groups   Name        Variance Std.Dev.
 id       (Intercept)  2.262   1.504
 Residual             13.082   3.617
Number of obs: 4284, groups:  id, 46
```

```
Fixed effects:
            Estimate Std. Error      df t value Pr(>|t|)
(Intercept)  -6.9477     0.2312 45.4659  -30.05   <2e-16 ***
```

Table A3d. Intraclassencorrelation of the Data, Red Colour Channel

```
ICCbare(id, red, data)
[1] 0.1462976
Warning message:
In ICCbare(id, red, data) : Missing levels of 'x' have been removed
```

Table A3e. Variance in the Data Set, Blue Colour Channel

```
summary(lmer(blue ~ 1|id, data))
Linear mixed model fit by REML. t-tests use Satterthwaite's method
['lmerModLmerTest']
Formula: blue ~ 1 | id
   Data: data

REML criterion at convergence: 21846.9

Scaled residuals:
    Min      1Q  Median      3Q     Max
-7.7166 -0.6125  0.0368  0.6438  3.2987

Random effects:
 Groups   Name        Variance Std.Dev.
 id       (Intercept) 0.9735   0.9867
 Residual             9.3688   3.0608
Number of obs: 4284, groups:  id, 46

Fixed effects:
            Estimate Std. Error      df t value Pr(>|t|)
(Intercept)  -8.0504     0.1553 44.5009  -51.82   <2e-16 ***
```

Table A3f. Intraclassencorrelation of the Data, Blue Colour Channel

```
ICCbare(id, blue, data)
[1] 0.09243149
Warning message:
In ICCbare(id, blue, data) : Missing levels of 'x' have been removed
```

Table A4a. Descriptive Properties of the Three Colour Channels.

```
mean_se(data$green, 1)
          y      ymin     ymax
1 -1.795557 -1.879863 -1.71125
mean_se(data$red, 1)
         y      ymin      ymax
1 -6.89545 -6.955146 -6.835755
mean_se(data$blue, 1)
          y     ymin      ymax
1 -7.945563 -7.99459 -7.896535
```

Table A4b. Simple Linear Model with Comparison of SNR in the Three Colour Channels

```
summary(x1<-lm(snr~channel, colourlong))

Call:
lm(formula = snr ~ channel, data = colourlong)

Residuals:
     Min       1Q   Median       3Q      Max
-27.5225  -2.5040   0.1532   2.7538  13.9350

Coefficients:
             Estimate Std. Error t value Pr(>|t|)
(Intercept)  -6.85682    0.03188 -215.10   <2e-16 ***
channelgreen  4.63357    0.04508  102.78   <2e-16 ***
channelblue  -1.01304    0.04508  -22.47   <2e-16 ***
```

Table A4c. Model with Comparison of SNR in the Three Colour Channels Using the Established Fitted Model Syntax

```
summary(lmer(snr~channel + (1|id/time), colourlong))
boundary (singular) fit: see ?isSingular
Linear mixed model fit by REML. t-tests use Satterthwaite's method
['lmerModLmerTest']
Formula: snr ~ channel + (1 | id/time)
   Data: colourlong

REML criterion at convergence: 281768.4

Scaled residuals:
    Min      1Q  Median      3Q     Max
-6.5012 -0.6004  0.0644  0.6775  4.1243

Random effects:
 Groups   Name        Variance Std.Dev.
 time:id  (Intercept)  7.405   2.721
 id       (Intercept)  0.000   0.000
 Residual             10.675   3.267
Number of obs: 53976, groups:  time:id, 140; id, 49

Fixed effects:
               Estimate Std. Error         df t value Pr(>|t|)
(Intercept)  -6.857e+00  2.314e-01  1.412e+02  -29.64   <2e-16 ***
channelgreen  4.634e+00  3.445e-02  5.383e+04  134.51   <2e-16 ***
channelblue  -1.013e+00  3.445e-02  5.383e+04  -29.41   <2e-16 ***
```

Table A5a. Generic Linear Model based on the Study Data

```
summary(x1 <- nlme::gls(green~1, meth="ML", data))
Generalized least squares fit by maximum likelihood
  Model: green ~ 1
  Data: data
```

```
       AIC      BIC    logLik
  26794.82 26807.54 -13395.41

Coefficients:
                Value  Std.Error   t-value p-value
(Intercept) -1.795557 0.08430644 -21.29798       0

Standardized residuals:
       Min         Q1        Med         Q3        Max
-4.5384585 -0.6672240  0.1139483  0.7449996  2.0643253

Residual standard error: 5.517404
Degrees of freedom: 4284 total; 4283 residual
```

Table A5b: Generic Linear Mixed-Effects Model based on the Study Data

```
summary(x2 <- nlme::lme(green~1, random = ~1|id/time, data, meth="ML"))
Linear mixed-effects model fit by maximum likelihood
 Data: data
       AIC      BIC    logLik
  21945.23 21970.68 -10968.61

Random effects:
 Formula: ~1 | id
        (Intercept)
StdDev: 0.003831871

 Formula: ~1 | time %in% id
        (Intercept) Residual
StdDev:    4.636758 2.926598

Fixed effects: green ~ 1
                Value Std.Error   DF   t-value p-value
(Intercept) -1.859852 0.4036529 4150 -4.607554       0

Standardized Within-Group Residuals:
       Min         Q1        Med         Q3        Max
-6.3468982 -0.4836380  0.0712910  0.5842332  3.7580586

Number of Observations: 4284
Number of Groups:
          id time %in% id
          46          134
```

Table A5c. Likelihood Ratio Test of the Two Generic Models with and without Mixed-Effects

```
anova(x1,x2)
   Model df      AIC      BIC    logLik   Test  L.Ratio p-value
x1     1  2 26794.82 26807.54 -13395.41
x2     2  4 21945.23 21970.68 -10968.61 1 vs 2 4853.588  <.0001
```

Table A6a/A9b/A15a. SNR in the Green Colour Channel

```
summary( green1<- lmer ( green ~ time + ( 1 | id / time ), data))
Linear mixed model fit by REML. t-tests use Satterthwaite's method
['lmerModLmerTest']
Formula: green ~ time + (1 | id/time)
   Data: data

REML criterion at convergence: 21876

Scaled residuals:
    Min      1Q  Median      3Q     Max
-6.3590 -0.4845  0.0717  0.5826  3.7332

Random effects:
 Groups   Name        Variance Std.Dev.
 time:id  (Intercept) 11.709   3.422
 id       (Intercept)  3.307   1.818
 Residual              8.565   2.927
Number of obs: 4284, groups:  time:id, 134; id, 46

Fixed effects:
            Estimate Std. Error       df t value Pr(>|t|)
(Intercept)   2.0209     0.6481 124.1588   3.118  0.00226 **
time2        -7.3574     0.8270  94.1807  -8.896 4.02e-14 ***
time3        -4.4419     0.9500  96.8520  -4.676 9.48e-06 ***
time4        -3.8851     0.8208  93.7500  -4.733 7.81e-06 ***
```

Table A6b. SNR in the Green Colour Channel with Forward Difference Coding

```
summary( green3 <- lmer ( green ~ diff.time + ( 1 | id / time ), data))
Linear mixed model fit by REML. t-tests use Satterthwaite's method
['lmerModLmerTest']
Formula: green ~ diff.time + (1 | id/time)
   Data: data

REML criterion at convergence: 21876

Scaled residuals:
    Min      1Q  Median      3Q     Max
-6.3590 -0.4845  0.0717  0.5826  3.7332

Random effects:
 Groups   Name        Variance Std.Dev.
 time:id  (Intercept) 11.709   3.422
 id       (Intercept)  3.307   1.818
 Residual              8.565   2.927
Number of obs: 4284, groups:  time:id, 134; id, 46

Fixed effects:
             Estimate Std. Error      df t value Pr(>|t|)
(Intercept)   -1.9002     0.4151 41.6290  -4.577 4.21e-05 ***
diff.time2-1  -7.3574     0.8270 94.1807  -8.896 4.02e-14 ***
diff.time3-2   2.9155     0.9462 98.0546   3.081  0.00268 **
diff.time4-3   0.5568     0.9399 97.2471   0.592  0.55495
```

Table A7a. SNR in the Red Colour Channel

```
summary( red1<- lmer ( red ~ time + ( 1 | id / time ), data))
Linear mixed model fit by REML. t-tests use Satterthwaite's method
['lmerModLmerTest']
Formula: red ~ time + (1 | id/time)
   Data: data

REML criterion at convergence: 21372.5

Scaled residuals:
    Min      1Q  Median      3Q     Max
-5.5003 -0.5932  0.0663  0.6571  3.1796

Random effects:
 Groups   Name        Variance Std.Dev.
 time:id  (Intercept) 3.8903   1.9724
 id       (Intercept) 0.8489   0.9214
 Residual             7.8519   2.8021
Number of obs: 4284, groups:  time:id, 134; id, 46

Fixed effects:
            Estimate Std. Error       df t value Pr(>|t|)
(Intercept)  -4.4284     0.3727 128.4959 -11.883  < 2e-16 ***
time2        -4.3145     0.4860  98.2820  -8.878 3.21e-14 ***
time3        -3.2854     0.5576 101.6461  -5.892 4.98e-08 ***
time4        -2.3430     0.4828  98.2967  -4.853 4.57e-06 ***
```

Table A7b. SNR in the Red Colour Channel with Forward Difference Coding

```
summary( red3 <- lmer ( red ~ diff.time + ( 1 | id / time ), data))
Linear mixed model fit by REML. t-tests use Satterthwaite's method
['lmerModLmerTest']
Formula: red ~ diff.time + (1 | id/time)
   Data: data

REML criterion at convergence: 21372.5

Scaled residuals:
    Min      1Q  Median      3Q     Max
-5.5003 -0.5932  0.0663  0.6571  3.1796

Random effects:
 Groups   Name        Variance Std.Dev.
 time:id  (Intercept) 3.8903   1.9724
 id       (Intercept) 0.8489   0.9214
 Residual             7.8519   2.8021
Number of obs: 4284, groups:  time:id, 134; id, 46

Fixed effects:
             Estimate Std. Error       df t value Pr(>|t|)
(Intercept)   -6.9141     0.2302  44.2037 -30.041  < 2e-16 ***
diff.time2-1  -4.3145     0.4860  98.2820  -8.878 3.21e-14 ***
diff.time3-2   1.0290     0.5547 102.3055   1.855   0.0664 .
```

```
diff.time4-3   0.9424     0.5515 101.8693   1.709   0.0905 .
```

Table A7c. SNR in the Red Colour Channel with Time = 2 as a Reference Level

```
summary( red1<- lmer ( red ~ time + ( 1 | id / time ), data))
Linear mixed model fit by REML. t-tests use Satterthwaite's method
['lmerModLmerTest']
Formula: red ~ time + (1 | id/time)
   Data: data

REML criterion at convergence: 21372.5

Scaled residuals:
    Min      1Q  Median      3Q     Max
-5.5003 -0.5932  0.0663  0.6571  3.1796

Random effects:
 Groups   Name        Variance Std.Dev.
 time:id  (Intercept) 3.8903   1.9724
 id       (Intercept) 0.8489   0.9214
 Residual             7.8519   2.8021
Number of obs: 4284, groups:  time:id, 134; id, 46

Fixed effects:
            Estimate Std. Error       df t value Pr(>|t|)
(Intercept)  -8.7429     0.3668 126.6654 -23.839  < 2e-16 ***
time1         4.3145     0.4860  98.2820   8.878 3.21e-14 ***
time3         1.0290     0.5547 102.3055   1.855   0.0664 .
time4         1.9714     0.4793  98.9041   4.113 8.08e-05 ***
```

Table A8a. SNR in the Blue Colour Channel

```
summary( blue1<- lmer ( blue ~ time + ( 1 | id / time ), data))
Linear mixed model fit by REML. t-tests use Satterthwaite's method
['lmerModLmerTest']
Formula: blue ~ time + (1 | id/time)
   Data: data

REML criterion at convergence: 20778.3

Scaled residuals:
    Min      1Q  Median      3Q     Max
-7.9790 -0.6005  0.0477  0.6724  2.8813

Random effects:
 Groups   Name        Variance Std.Dev.
 time:id  (Intercept) 2.69408  1.6414
 id       (Intercept) 0.07874  0.2806
 Residual             6.90745  2.6282
Number of obs: 4284, groups:  time:id, 134; id, 46

Fixed effects:
            Estimate Std. Error       df t value Pr(>|t|)
(Intercept)  -6.8572     0.2908 132.4400 -23.584  < 2e-16 ***
```

```
time2        -2.1000     0.4033 104.1321  -5.207 9.72e-07 ***
time3        -0.9527     0.4603 109.8288  -2.070  0.04084 *
time4        -1.2372     0.4011 104.1703  -3.085  0.00261 **
```

Table A8b. SNR in the Blue Colour Channel with Forward Difference Coding

```
summary( blue3 <- lmer ( blue ~ diff.time + ( 1 | id / time ), data))
Linear mixed model fit by REML. t-tests use Satterthwaite's method
['lmerModLmerTest']
Formula: blue ~ diff.time + (1 | id/time)
   Data: data

REML criterion at convergence: 20778.3

Scaled residuals:
    Min      1Q  Median      3Q     Max
-7.9790 -0.6005  0.0477  0.6724  2.8813

Random effects:
 Groups   Name        Variance Std.Dev.
 time:id  (Intercept) 2.69408  1.6414
 id       (Intercept) 0.07874  0.2806
 Residual             6.90745  2.6282
Number of obs: 4284, groups:  time:id, 134; id, 46

Fixed effects:
             Estimate Std. Error       df t value Pr(>|t|)
(Intercept)   -7.9297     0.1579  45.4323 -50.232  < 2e-16 ***
diff.time2-1  -2.1000     0.4033 104.1321  -5.207 9.72e-07 ***
diff.time3-2   1.1472     0.4572 109.6841   2.509   0.0136 *
diff.time4-3  -0.2845     0.4552 109.2983  -0.625   0.5332
```

Table A8c. SNR in the Blue Colour Channel with Time = 2 as a Reference Level

```
summary( blue1<- lmer ( blue ~ time + ( 1 | id / time ), data))
Linear mixed model fit by REML. t-tests use Satterthwaite's method
['lmerModLmerTest']
Formula: blue ~ time + (1 | id/time)
   Data: data

REML criterion at convergence: 20778.3

Scaled residuals:
    Min      1Q  Median      3Q     Max
-7.9790 -0.6005  0.0477  0.6724  2.8813

Random effects:
 Groups   Name        Variance Std.Dev.
 time:id  (Intercept) 2.69409  1.6414
 id       (Intercept) 0.07874  0.2806
 Residual             6.90745  2.6282
Number of obs: 4284, groups:  time:id, 134; id, 46

Fixed effects:
```

```
            Estimate Std. Error       df t value Pr(>|t|)
(Intercept)  -8.9572     0.2856 130.0388 -31.361  < 2e-16 ***
time1         2.1000     0.4033 104.1314   5.207 9.72e-07 ***
time3         1.1472     0.4572 109.6836   2.509   0.0136 *
time4         0.8627     0.3975 103.8813   2.170   0.0323 *
```

Table A9a. Basic Model with the Time of the Measurement Nested on the Subjects' (Patients') Level

```
summary(v1 <- lmer ( green ~ ( 1 | id/time), data))
boundary (singular) fit: see ?isSingular
Linear mixed model fit by REML. t-tests use Satterthwaite's method
['lmerModLmerTest']
Formula: green ~ (1 | id/time)
   Data: data

REML criterion at convergence: 21937.2

Scaled residuals:
    Min      1Q  Median      3Q     Max
-6.3468 -0.4837  0.0712  0.5842  3.7582

Random effects:
 Groups   Name        Variance  Std.Dev.
 time:id  (Intercept) 2.166e+01 4.654e+00
 id       (Intercept) 4.685e-09 6.845e-05
 Residual             8.565e+00 2.927e+00
Number of obs: 4284, groups:  time:id, 134; id, 46

Fixed effects:
            Estimate Std. Error       df t value Pr(>|t|)
(Intercept)  -1.8599     0.4051 133.1983  -4.591 1.01e-05 ***
```

Table A9c. Model without Coded Interaction Between the Time of the Measurement and the Chest Side

```
summary(v3<- lmer(green ~ time + ita + (1|id/time), data))
Linear mixed model fit by REML. t-tests use Satterthwaite's method
['lmerModLmerTest']
Formula: green ~ time + ita + (1 | id/time)
   Data: data

REML criterion at convergence: 21797.5

Scaled residuals:
    Min      1Q  Median      3Q     Max
-6.5590 -0.4612  0.0767  0.5731  3.9092

Random effects:
 Groups   Name        Variance Std.Dev.
 time:id  (Intercept) 11.715   3.423
 id       (Intercept)  3.306   1.818
 Residual              8.401   2.898
Number of obs: 4284, groups:  time:id, 134; id, 46
```

```
Fixed effects:
             Estimate Std. Error         df t value Pr(>|t|)
(Intercept)   2.42251    0.64956  125.33348   3.729 0.000289 ***
time2        -7.35697    0.82702   94.16987  -8.896 4.04e-14 ***
time3        -4.44199    0.94998   96.84197  -4.676 9.48e-06 ***
time4        -3.88503    0.82084   93.73402  -4.733 7.82e-06 ***
itaITA       -0.80366    0.08856 4149.01313  -9.074  < 2e-16 ***
```

Table A9d/A10a. Model with Coded Interaction Between the Time of the Measurement and the Chest Side

```
summary(v4<- lmer(green ~ time * ita + (1|id/time), data))
Linear mixed model fit by REML. t-tests use Satterthwaite's method
['lmerModLmerTest']
Formula: green ~ time * ita + (1 | id/time)
   Data: data

REML criterion at convergence: 21761.5

Scaled residuals:
    Min      1Q  Median      3Q     Max
-6.4572 -0.4695  0.0765  0.5780  4.0176

Random effects:
 Groups   Name        Variance Std.Dev.
 time:id  (Intercept) 11.718   3.423
 id       (Intercept)  3.307   1.818
 Residual              8.327   2.886
Number of obs: 4284, groups:  time:id, 134; id, 46

Fixed effects:
                Estimate  Std. Error      df   t value Pr(>|t|)
(Intercept)       1.8872     0.6538  128.5811   2.887  0.00457 **
time2            -7.8493     0.8355   98.1006  -9.395 2.47e-15 ***
time3            -4.3341     0.9597  100.8573  -4.516 1.71e-05 ***
time4            -4.4154     0.8297   97.8377  -5.322 6.52e-07 ***
itaother          0.2670     0.1723 4146.0136   1.549  0.12137
time2:itaother    0.9849     0.2375 4146.0136   4.146 3.45e-05 ***
time3:itaother   -0.2161     0.2720 4146.0136  -0.794  0.42704
time4:itaother    1.0606     0.2415 4146.0136   4.393 1.15e-05 ***
```

Table A9e. Comparing Alternative Models with and without a Coded Interaction Between the Time of the Measurement and the Chest Side

```
anova (v1, v2, v3, v4)
refitting model(s) with ML (instead of REML)
Data: data
Models:
v1: green ~ (1 | id/time)
v2: green ~ time + (1 | id/time)
v3: green ~ time + ita + (1 | id/time)
v4: green ~ time * ita + (1 | id/time)
```

```
   npar   AIC   BIC logLik deviance  Chisq Df Pr(>Chisq)
v1    4 21945 21971 -10969    21937
v2    7 21894 21939 -10940    21880 57.205  3  2.324e-12 ***
v3    8 21815 21865 -10899    21799 81.556  1  < 2.2e-16 ***
v4   11 21781 21851 -10880    21759 39.453  3  1.392e-08 ***
```

Table A9f. Comparing the Models with and without Chest Side as a Fixed Effect (Summary of the Models above)

```
anova ( v2, v4)
refitting model(s) with ML (instead of REML)
Data: data
Models:
v2: green ~ time + (1 | id/time)
v4: green ~ time * ita + (1 | id/time)
   npar   AIC   BIC logLik deviance  Chisq Df Pr(>Chisq)
v2    7 21894 21939 -10940    21880
v4   11 21781 21851 -10880    21759 121.01  4  < 2.2e-16 ***
```

Table A10b. 0 Intercept Model for Determining Side Differences of the SNR Values from the Green Colour Channel

```
summary(x4<-lmer(green~0 + time + time : ita + (1|id/time), data))
Linear mixed model fit by REML. t-tests use Satterthwaite's method
['lmerModLmerTest']
Formula: green ~ 0 + time + time:ita + (1 | id/time)
   Data: data

REML criterion at convergence: 21761.5

Scaled residuals:
    Min      1Q  Median      3Q     Max
-6.4572 -0.4695  0.0765  0.5780  4.0176

Random effects:
 Groups   Name        Variance Std.Dev.
 time:id  (Intercept) 11.718   3.423
 id       (Intercept)  3.307   1.818
 Residual              8.327   2.886
Number of obs: 4284, groups:  time:id, 134; id, 46

Fixed effects:
               Estimate  Std. Error      df   t value Pr(>|t|)
time1            1.8872     0.6538  128.5811   2.887  0.00457 **
time2           -5.9621     0.6443  127.3295  -9.254 6.61e-16 ***
time3           -2.4470     0.8059  134.0733  -3.036  0.00288 **
time4           -2.5283     0.6372  127.1295  -3.968  0.00012 ***
time1:itaother   0.2670     0.1723 4146.0136   1.549  0.12137
time2:itaother   1.2518     0.1635 4146.0136   7.656 2.36e-14 ***
time3:itaother   0.0509     0.2105 4146.0136   0.242  0.80892
time4:itaother   1.3276     0.1692 4146.0136   7.848 5.34e-15 ***
```

Table A11a. Fitted Model for SNR Values from the Green Colour Channel with Forward Difference Coding

```
summary(x5<-lmer(green ~ diff.time * ita + (1|id/time), data))
Linear mixed model fit by REML. t-tests use Satterthwaite's method
['lmerModLmerTest']
Formula: green ~ diff.time * ita + (1 | id/time)
   Data: data

REML criterion at convergence: 21761.5

Scaled residuals:
    Min      1Q  Median      3Q     Max
-6.4572 -0.4695  0.0765  0.5780  4.0176

Random effects:
 Groups   Name        Variance Std.Dev.
 time:id  (Intercept) 11.718   3.423
 id       (Intercept)  3.307   1.818
 Residual              8.327   2.886
Number of obs: 4284, groups:  time:id, 134; id, 46

Fixed effects:
                     Estimate Std. Error       df t value Pr(>|t|)
(Intercept)           -2.26255 0.41757   42.61527 -5.418 2.61e-06***
diff.time2-1          -7.84929 0.83549   98.10061 -9.395 2.47e-15***
diff.time3-2           3.51518 0.95556  101.98266  3.679 0.000376***
diff.time4-3          -0.08131 0.94955  101.29597 -0.086 0.931928
itaother               0.72431 0.08991 4146.01363  8.056 1.02e-15***
diff.time2-1:itaother  0.98487 0.23753 4146.01363  4.146 3.45e-05***
diff.time3-2:itaother -1.20092 0.26651 4146.01363 -4.506 6.78e-06***
diff.time4-3:itaother  1.27669 0.27002 4146.01363  4.728 2.34e-06***
```

Table A12. Extended Model with Cofactors Added

```
summary(x1 <- lmer(green ~ time * ita + (1|id/time) + age + height + rhythm
+ sex + weight, data))
Linear mixed model fit by REML. t-tests use Satterthwaite's method
['lmerModLmerTest']
Formula: green ~ time * ita + (1 | id/time) + age + height + rhythm + sex +
weight
   Data: data

REML criterion at convergence: 21598.7

Scaled residuals:
    Min      1Q  Median      3Q     Max
-6.4477 -0.4672  0.0763  0.5785  4.0126

Random effects:
 Groups   Name        Variance Std.Dev.
 time:id  (Intercept) 11.800   3.435
 id       (Intercept)  4.123   2.031
 Residual              8.351   2.890
Number of obs: 4248, groups:  time:id, 133; id, 46
```

```
Fixed effects:
                 Estimate Std. Error         df t value Pr(>|t|)
(Intercept)     1.278e+01  1.469e+01  4.129e+01   0.870 0.389395
time2          -7.929e+00  1.205e+00  1.088e+02  -6.580 1.70e-09 ***
time3          -4.358e+00  1.107e+00  1.065e+02  -3.936 0.000148 ***
time4          -4.480e+00  8.402e-01  9.464e+01  -5.332 6.58e-07 ***
itaother        2.670e-01  1.725e-01  4.111e+03   1.547 0.121908
age            -3.118e-02  6.966e-02  3.465e+01  -0.448 0.657291
height         -5.217e-02  8.099e-02  4.121e+01  -0.644 0.523017
rhythm          3.282e-02  5.183e-01  1.225e+02   0.063 0.949613
sexW           -4.346e-01  2.323e+00  3.433e+01  -0.187 0.852677
weight          5.504e-03  3.762e-02  4.340e+01   0.146 0.884358
time2:itaother  1.023e+00  2.395e-01  4.111e+03   4.271 1.99e-05 ***
time3:itaother -2.161e-01  2.724e-01  4.111e+03  -0.793 0.427705
time4:itaother  1.061e+00  2.418e-01  4.111e+03   4.386 1.18e-05 ***
```

Table A13a/A14a. Altered Fitted Model with ROIs 1-3 and 5-7 Instead of Chest Side

```
summary (x1 <-lmer (green ~ time * roi + (1 | id/time), d2x))
Linear mixed model fit by REML. t-tests use Satterthwaite's method
['lmerModLmerTest']
Formula: green ~ time * roi + (1 | id/time)
   Data: d2x

REML criterion at convergence: 66426.1

Scaled residuals:
    Min      1Q  Median      3Q     Max
-6.5306 -0.5278  0.0740  0.6162  3.2913

Random effects:
 Groups   Name        Variance Std.Dev.
 time:id  (Intercept) 10.399   3.225
 id       (Intercept)  2.877   1.696
 Residual              9.781   3.127
Number of obs: 12852, groups:  time:id, 134; id, 46

Fixed effects:
             Estimate Std. Error         df t value Pr(>|t|)
(Intercept)    1.8270     0.6174   134.5688   2.959  0.00365 **
time2         -6.9383     0.7910   104.6899  -8.772 3.52e-14 ***
time3         -3.9766     0.9085   107.5002  -4.377 2.80e-05 ***
time4         -4.0151     0.7858   104.5363  -5.110 1.46e-06 ***
roi2          -0.2674     0.1867 12698.1085  -1.432  0.15215
roi3          -1.0932     0.1867 12698.1085  -5.854 4.92e-09 ***
roi5          -0.7550     0.1867 12698.1085  -4.043 5.31e-05 ***
roi6          -0.8371     0.1867 12698.1085  -4.483 7.43e-06 ***
roi7          -0.5936     0.1867 12698.1085  -3.179  0.00148 **
time2:roi2     0.4401     0.2574 12698.1085   1.710  0.08733 .
time3:roi2    -0.1410     0.2948 12698.1085  -0.478  0.63245
time4:roi2     0.4609     0.2617 12698.1085   1.761  0.07825 .
time2:roi3     1.3818     0.2574 12698.1085   5.368 8.12e-08 ***
time3:roi3    -0.1409     0.2948 12698.1085  -0.478  0.63277
```

```
time4:roi3      0.5035     0.2617 12698.1085   1.924  0.05437 .
time2:roi5      0.3070     0.2574 12698.1085   1.193  0.23302
time3:roi5      1.3885     0.2948 12698.1085   4.710 2.50e-06 ***
time4:roi5      1.0221     0.2617 12698.1085   3.906 9.45e-05 ***
time2:roi6     -0.3903     0.2574 12698.1085  -1.516  0.12949
time3:roi6      0.4335     0.2948 12698.1085   1.470  0.14146
time4:roi6     -0.3939     0.2617 12698.1085  -1.505  0.13233
time2:roi7     -0.5495     0.2574 12698.1085  -2.134  0.03282 *
time3:roi7     -1.6201     0.2948 12698.1085  -5.496 3.96e-08 ***
time4:roi7     -2.3849     0.2617 12698.1085  -9.114  < 2e-16 ***
```

Table A13b/A14b. Altered Fitted Model with ROIs 1-3 and 5-7 Instead of Chest Side, forward difference coding, reference at ROI 1

```
summary(x4 <- lmer ( green ~ diff.time * roi + (1 | id / time), d2x))
Linear mixed model fit by REML. t-tests use Satterthwaite's method
['lmerModLmerTest']
Formula: green ~ diff.time * roi + (1 | id/time)
   Data: d2x

REML criterion at convergence: 66426.1

Scaled residuals:
    Min      1Q  Median      3Q     Max
-6.5306 -0.5278  0.0740  0.6162  3.2913

Random effects:
 Groups   Name        Variance Std.Dev.
 time:id  (Intercept) 10.399   3.225
 id       (Intercept)  2.877   1.696
 Residual              9.781   3.127
Number of obs: 12852, groups:  time:id, 134; id, 46

Fixed effects:
                    Estimate Std. Error         df t value Pr(>|t|)
(Intercept)       -1.905e+00  3.928e-01  4.551e+01  -4.851 1.48e-05 ***
diff.time2-1      -6.938e+00  7.910e-01  1.047e+02  -8.772 3.52e-14 ***
diff.time3-2       2.962e+00  9.045e-01  1.086e+02   3.274 0.001421 **
diff.time4-3      -3.853e-02  8.991e-01  1.080e+02  -0.043 0.965894
roi2              -7.742e-02  9.744e-02  1.270e+04  -0.795 0.426911
roi3              -6.571e-01  9.744e-02  1.270e+04  -6.743 1.62e-11 ***
roi5              -7.557e-02  9.744e-02  1.270e+04  -0.776 0.438016
roi6              -9.248e-01  9.744e-02  1.270e+04  -9.491  < 2e-16 ***
roi7              -1.732e+00  9.744e-02  1.270e+04 -17.777  < 2e-16 ***
diff.time2-1:roi2  4.401e-01  2.574e-01  1.270e+04   1.710 0.087334 .
diff.time3-2:roi2 -5.811e-01  2.888e-01  1.270e+04  -2.012 0.044243 *
diff.time4-3:roi2  6.018e-01  2.926e-01  1.270e+04   2.057 0.039744 *
diff.time2-1:roi3  1.382e+00  2.574e-01  1.270e+04   5.368 8.12e-08 ***
diff.time3-2:roi3 -1.523e+00  2.888e-01  1.270e+04  -5.272 1.37e-07 ***
diff.time4-3:roi3  6.444e-01  2.926e-01  1.270e+04   2.202 0.027691 *
diff.time2-1:roi5  3.070e-01  2.574e-01  1.270e+04   1.193 0.233023
diff.time3-2:roi5  1.081e+00  2.888e-01  1.270e+04   3.744 0.000182 ***
diff.time4-3:roi5 -3.664e-01  2.926e-01  1.270e+04  -1.252 0.210542
diff.time2-1:roi6 -3.903e-01  2.574e-01  1.270e+04  -1.516 0.129494
```

```
diff.time3-2:roi6  8.238e-01  2.888e-01  1.270e+04   2.852 0.004351 **
diff.time4-3:roi6 -8.273e-01  2.926e-01  1.270e+04  -2.827 0.004704 **
diff.time2-1:roi7 -5.495e-01  2.574e-01  1.270e+04  -2.134 0.032824 *
diff.time3-2:roi7 -1.071e+00  2.888e-01  1.270e+04  -3.707 0.000211 ***
diff.time4-3:roi7 -7.648e-01  2.926e-01  1.270e+04  -2.613 0.008976 **
```

Table A13c. Altered Fitted Model with ROIs 1-3 and 5-7 Instead of Chest Side. Reference at ROI = 6 and time = 3.

```
summary (x1 <-lmer (green ~ time * roi + (1 | id/time), d2x))
Linear mixed model fit by REML. t-tests use Satterthwaite's method
['lmerModLmerTest']
Formula: green ~ time * roi + (1 | id/time)
   Data: d2x

REML criterion at convergence: 66426.1

Scaled residuals:
    Min      1Q  Median      3Q     Max
-6.5306 -0.5278  0.0740  0.6162  3.2913

Random effects:
 Groups   Name        Variance Std.Dev.
 time:id  (Intercept) 10.399   3.225
 id       (Intercept)  2.877   1.696
 Residual              9.781   3.127
Number of obs: 12852, groups:  time:id, 134; id, 46

Fixed effects:
             Estimate Std. Error         df t value Pr(>|t|)
(Intercept) -2.553e+00  7.614e-01  1.401e+02  -3.353 0.001028 **
time1        3.543e+00  9.085e-01  1.075e+02   3.900 0.000168 ***
time2       -3.785e+00  9.045e-01  1.086e+02  -4.185 5.81e-05 ***
time4       -8.659e-01  8.991e-01  1.080e+02  -0.963 0.337685
roi5         1.037e+00  2.281e-01  1.270e+04   4.547 5.49e-06 ***
roi7        -1.810e+00  2.281e-01  1.270e+04  -7.936 2.27e-15 ***
roi1         4.036e-01  2.281e-01  1.270e+04   1.770 0.076833 .
roi2        -4.796e-03  2.281e-01  1.270e+04  -0.021 0.983225
roi3        -8.304e-01  2.281e-01  1.270e+04  -3.641 0.000273 ***
time1:roi5  -9.550e-01  2.948e-01  1.270e+04  -3.240 0.001200 **
time2:roi5  -2.577e-01  2.888e-01  1.270e+04  -0.892 0.372357
time4:roi5   4.609e-01  2.926e-01  1.270e+04   1.575 0.115286
time1:roi7   2.054e+00  2.948e-01  1.270e+04   6.966 3.41e-12 ***
time2:roi7   1.894e+00  2.888e-01  1.270e+04   6.559 5.63e-11 ***
time4:roi7   6.255e-02  2.926e-01  1.270e+04   0.214 0.830751
time1:roi1   4.335e-01  2.948e-01  1.270e+04   1.470 0.141460
time2:roi1   8.238e-01  2.888e-01  1.270e+04   2.852 0.004351 **
time4:roi1   8.273e-01  2.926e-01  1.270e+04   2.827 0.004704 **
time1:roi2   5.745e-01  2.948e-01  1.270e+04   1.949 0.051347 .
time2:roi2   1.405e+00  2.888e-01  1.270e+04   4.864 1.16e-06 ***
time4:roi2   1.429e+00  2.926e-01  1.270e+04   4.884 1.05e-06 ***
time1:roi3   5.743e-01  2.948e-01  1.270e+04   1.948 0.051399 .
time2:roi3   2.346e+00  2.888e-01  1.270e+04   8.124 4.94e-16 ***
time4:roi3   1.472e+00  2.926e-01  1.270e+04   5.029 5.00e-07 ***
```

Table A13d. Altered Fitted Model with ROIs 1-3 and 5-7 Instead of Chest Side. Reference at ROI = 6 and time = 4.

```
summary (x1 <-lmer (green ~ time * roi + (1 | id/time), d2x))
Linear mixed model fit by REML. t-tests use Satterthwaite's method
['lmerModLmerTest']
Formula: green ~ time * roi + (1 | id/time)
   Data: d2x

REML criterion at convergence: 66426.1

Scaled residuals:
    Min      1Q  Median      3Q     Max
-6.5306 -0.5278  0.0740  0.6162  3.2913

Random effects:
 Groups   Name        Variance Std.Dev.
 time:id  (Intercept) 10.399   3.225
 id       (Intercept)  2.877   1.696
 Residual              9.781   3.127
Number of obs: 12852, groups:  time:id, 134; id, 46

Fixed effects:
              Estimate Std. Error         df t value Pr(>|t|)
(Intercept) -3.419e+00  6.019e-01  1.334e+02  -5.680 8.08e-08 ***
time1        4.409e+00  7.858e-01  1.045e+02   5.611 1.66e-07 ***
time2       -2.920e+00  7.807e-01  1.056e+02  -3.739 0.000300 ***
time3        8.659e-01  8.991e-01  1.080e+02   0.963 0.337685
roi5         1.498e+00  1.833e-01  1.270e+04   8.171 3.35e-16 ***
roi7        -1.748e+00  1.833e-01  1.270e+04  -9.532  < 2e-16 ***
roi1         1.231e+00  1.833e-01  1.270e+04   6.714 1.97e-11 ***
roi2         1.424e+00  1.833e-01  1.270e+04   7.769 8.50e-15 ***
roi3         6.413e-01  1.833e-01  1.270e+04   3.498 0.000471 ***
time1:roi5  -1.416e+00  2.617e-01  1.270e+04  -5.411 6.39e-08 ***
time2:roi5  -7.186e-01  2.550e-01  1.270e+04  -2.818 0.004836 **
time3:roi5  -4.609e-01  2.926e-01  1.270e+04  -1.575 0.115286
time1:roi7   1.991e+00  2.617e-01  1.270e+04   7.608 2.97e-14 ***
time2:roi7   1.832e+00  2.550e-01  1.270e+04   7.185 7.11e-13 ***
time3:roi7  -6.255e-02  2.926e-01  1.270e+04  -0.214 0.830751
time1:roi1  -3.939e-01  2.617e-01  1.270e+04  -1.505 0.132330
time2:roi1  -3.549e-03  2.550e-01  1.270e+04  -0.014 0.988895
time3:roi1  -8.273e-01  2.926e-01  1.270e+04  -2.827 0.004704 **
time1:roi2  -8.547e-01  2.617e-01  1.270e+04  -3.266 0.001093 **
time2:roi2  -2.426e-02  2.550e-01  1.270e+04  -0.095 0.924195
time3:roi2  -1.429e+00  2.926e-01  1.270e+04  -4.884 1.05e-06 ***
time1:roi3  -8.974e-01  2.617e-01  1.270e+04  -3.429 0.000608 ***
time2:roi3   8.747e-01  2.550e-01  1.270e+04   3.431 0.000604 ***
time3:roi3  -1.472e+00  2.926e-01  1.270e+04  -5.029 5.00e-07 ***
```

Table A13e. Altered Fitted Model with ROIs 1-3 and 5-7 Instead of Chest Side. Reference at ROI = 2 and time = 3.

```
summary (x1 <-lmer (green ~ time * roi + (1 | id/time), d2x))
```

```
Linear mixed model fit by REML. t-tests use Satterthwaite's method
['lmerModLmerTest']
Formula: green ~ time * roi + (1 | id/time)
   Data: d2x

REML criterion at convergence: 66426.1

Scaled residuals:
    Min      1Q  Median      3Q     Max
-6.5306 -0.5278  0.0740  0.6162  3.2913

Random effects:
 Groups   Name        Variance Std.Dev.
 time:id  (Intercept) 10.399   3.225
 id       (Intercept)  2.877   1.696
 Residual              9.781   3.127
Number of obs: 12852, groups:  time:id, 134; id, 46

Fixed effects:
              Estimate Std. Error         df t value Pr(>|t|)
(Intercept) -2.558e+00  7.614e-01  1.401e+02  -3.359 0.001006 **
time1        4.118e+00  9.085e-01  1.075e+02   4.532 1.52e-05 ***
time2       -2.381e+00  9.045e-01  1.086e+02  -2.632 0.009727 **
time4        5.633e-01  8.991e-01  1.080e+02   0.627 0.532293
roi1         4.084e-01  2.281e-01  1.270e+04   1.791 0.073392 .
roi3        -8.256e-01  2.281e-01  1.270e+04  -3.620 0.000296 ***
roi5         1.042e+00  2.281e-01  1.270e+04   4.568 4.97e-06 ***
roi6         4.796e-03  2.281e-01  1.270e+04   0.021 0.983225
roi7        -1.805e+00  2.281e-01  1.270e+04  -7.915 2.68e-15 ***
time1:roi1  -1.410e-01  2.948e-01  1.270e+04  -0.478 0.632453
time2:roi1  -5.811e-01  2.888e-01  1.270e+04  -2.012 0.044243 *
time4:roi1  -6.018e-01  2.926e-01  1.270e+04  -2.057 0.039744 *
time1:roi3  -1.298e-04  2.948e-01  1.270e+04   0.000 0.999649
time2:roi3   9.415e-01  2.888e-01  1.270e+04   3.260 0.001118 **
time4:roi3   4.251e-02  2.926e-01  1.270e+04   0.145 0.884493
time1:roi5  -1.529e+00  2.948e-01  1.270e+04  -5.188 2.15e-07 ***
time2:roi5  -1.663e+00  2.888e-01  1.270e+04  -5.756 8.80e-09 ***
time4:roi5  -9.683e-01  2.926e-01  1.270e+04  -3.309 0.000940 ***
time1:roi6  -5.745e-01  2.948e-01  1.270e+04  -1.949 0.051347 .
time2:roi6  -1.405e+00  2.888e-01  1.270e+04  -4.864 1.16e-06 ***
time4:roi6  -1.429e+00  2.926e-01  1.270e+04  -4.884 1.05e-06 ***
time1:roi7   1.479e+00  2.948e-01  1.270e+04   5.018 5.30e-07 ***
time2:roi7   4.895e-01  2.888e-01  1.270e+04   1.695 0.090133 .
time4:roi7  -1.367e+00  2.926e-01  1.270e+04  -4.670 3.04e-06 ***
```

Table A15b. Model without Coded Interaction Between the Time of the Measurement and the Surgical Technique Variable

```
summary (v2 <- lmer ( green ~ time + prep + (1 | id / time), data))
Linear mixed model fit by REML. t-tests use Satterthwaite's method
['lmerModLmerTest']
Formula: green ~ time + prep + (1 | id/time)
   Data: data
```

```
REML criterion at convergence: 21790.9

Scaled residuals:
    Min      1Q  Median      3Q     Max
-6.5368 -0.4621  0.0758  0.5664  3.8841

Random effects:
 Groups   Name        Variance Std.Dev.
 time:id  (Intercept) 11.733   3.425
 id       (Intercept)  3.380   1.838
 Residual              8.385   2.896
Number of obs: 4284, groups:  time:id, 134; id, 46

Fixed effects:
             Estimate Std. Error        df t value Pr(>|t|)
(Intercept)    1.7754     0.6536  126.6997   2.716  0.00752 **
time2         -7.3404     0.8278   93.8485  -8.867 4.76e-14 ***
time3         -4.4290     0.9510   96.4811  -4.657 1.02e-05 ***
time4         -3.8772     0.8216   93.4132  -4.719 8.30e-06 ***
prepSkel      -0.5423     0.1912 4185.2112  -2.836  0.00459 **
prepOther      0.6386     0.1059 4171.5554   6.030 1.78e-09 ***
```

Table A15c/A16. Model with Coded Interaction Between the Time of the Measurement and the Surgical Technique Variable

```
summary (v3 <- lmer ( green ~ time * prep + (1 | id / time), data))
Linear mixed model fit by REML. t-tests use Satterthwaite's method
['lmerModLmerTest']
Formula: green ~ time * prep + (1 | id/time)
   Data: data

REML criterion at convergence: 21738.7

Scaled residuals:
    Min      1Q  Median      3Q     Max
-6.3801 -0.4604  0.0732  0.5741  4.0383

Random effects:
 Groups   Name        Variance Std.Dev.
 time:id  (Intercept) 11.921   3.453
 id       (Intercept)  3.305   1.818
 Residual              8.285   2.878
Number of obs: 4284, groups:  time:id, 134; id, 46

Fixed effects:
                  Estimate Std. Error         df t value Pr(>|t|)
(Intercept)      1.848e+00  6.656e-01  1.345e+02   2.777 0.006278 **
time2           -7.471e+00  8.557e-01  1.039e+02  -8.731 4.57e-14 ***
time3           -3.725e+00  9.840e-01  1.078e+02  -3.786 0.000252 ***
time4           -4.430e+00  8.497e-01  1.039e+02  -5.213 9.49e-07 ***
prepSkel         1.636e-01  3.825e-01  4.244e+03   0.428 0.668979
prepOther        3.116e-01  2.011e-01  4.178e+03   1.550 0.121299
time2:prepSkel  -1.166e+00  5.148e-01  4.236e+03  -2.264 0.023630 *
time3:prepSkel  -1.853e+00  5.864e-01  4.234e+03  -3.160 0.001587 **
```

```
time4:prepSkel   3.593e-03  5.273e-01  4.233e+03   0.007 0.994563
time2:prepOther  6.154e-01  2.820e-01  4.184e+03   2.182 0.029133 *
time3:prepOther -8.044e-01  3.240e-01  4.185e+03  -2.483 0.013072 *
time4:prepOther  1.067e+00  2.845e-01  4.184e+03   3.749 0.000180 ***
```

Table A15d: Comparing Alternative Models with and without a Coded Interaction Between the Time of the Measurement and the Variable of the Surgical Technique

```
anova(v1,v2,v3)
refitting model(s) with ML (instead of REML)
Data: data
Models:
v1: green ~ time + (1 | id/time)
v2: green ~ time + prep + (1 | id/time)
v3: green ~ time * prep + (1 | id/time)
   npar   AIC   BIC logLik deviance  Chisq Df Pr(>Chisq)
v1    7 21894 21939 -10940    21880
v2    9 21808 21866 -10895    21790 89.576  2  < 2.2e-16 ***
v3   15 21766 21861 -10868    21736 54.531  6  5.766e-10 ***
```

Table A15e: Comparing Models with and without a Coded Interaction Between the Time of the Measurement and the Surgical Technique Variable

```
anova(v2,v3)
refitting model(s) with ML (instead of REML)
Data: data
Models:
v2: green ~ time + prep + (1 | id/time)
v3: green ~ time * prep + (1 | id/time)
   npar   AIC   BIC logLik deviance  Chisq Df Pr(>Chisq)
v2    9 21808 21866 -10895    21790
v3   15 21766 21861 -10868    21736 54.531  6  5.766e-10 ***
```

Table A16b. 0 Intercept Model with Coded Interaction Between the Time of the Measurement and Surgical Technique Variable for the Differences Between the Two Surgical techniques and the Other Side, Pedicled Technique as Reference

```
summary(x3<-lmer(green ~ 0 + time + time : prep + (1 | id / time), data))
Linear mixed model fit by REML. t-tests use Satterthwaite's method
['lmerModLmerTest']
Formula: green ~ 0 + time + time:prep + (1 | id/time)
   Data: data

REML criterion at convergence: 21738.7

Scaled residuals:
    Min      1Q  Median      3Q     Max
-6.3801 -0.4604  0.0732  0.5741  4.0383

Random effects:
 Groups   Name        Variance Std.Dev.
 time:id  (Intercept) 11.921   3.453
 id       (Intercept)  3.305   1.818
```

```
 Residual              8.285   2.878
Number of obs: 4284, groups:  time:id, 134; id, 46

Fixed effects:
                 Estimate Std. Error        df t value Pr(>|t|)
time1              1.8481     0.6656  134.4548   2.777 0.006278 **
time2             -5.6231     0.6588  135.4056  -8.535 2.51e-14 ***
time3             -1.8772     0.8250  142.8658  -2.275 0.024371 *
time4             -2.5819     0.6510  134.8151  -3.966 0.000118 ***
time1:prepSkel     0.1636     0.3825 4243.7767   0.428 0.668979
time2:prepSkel    -1.0020     0.3454 4245.4651  -2.901 0.003738 **
time3:prepSkel    -1.6896     0.4452 4245.5807  -3.795 0.000150 ***
time4:prepSkel     0.1672     0.3639 4249.5237   0.459 0.645996
time1:prepOther    0.3116     0.2010 4177.8660   1.550 0.121299
time2:prepOther    0.9269     0.1978 4184.0554   4.686 2.88e-06 ***
time3:prepOther   -0.4928     0.2542 4185.4985  -1.939 0.052572 .
time4:prepOther    1.3781     0.2014 4184.4657   6.841 8.99e-12 ***
```

Table A16c. 0 Intercept Model with Coded Interaction Between the Time of the Measurement and Surgical Technique Variable for the Differences Between the Two Surgical techniques and the Other Side, Skeletonised Technique as Reference

```
summary(x3<-lmer(green ~ 0 + time + time : prep + (1 | id / time), data))
Linear mixed model fit by REML. t-tests use Satterthwaite's method
['lmerModLmerTest']
Formula: green ~ 0 + time + time:prep + (1 | id/time)
   Data: data

REML criterion at convergence: 21738.7

Scaled residuals:
    Min      1Q  Median      3Q     Max
-6.3801 -0.4604  0.0732  0.5741  4.0383

Random effects:
 Groups   Name        Variance Std.Dev.
 time:id  (Intercept) 11.921   3.453
 id       (Intercept)  3.305   1.818
 Residual              8.285   2.878
Number of obs: 4284, groups:  time:id, 134; id, 46

Fixed effects:
                 Estimate Std. Error        df t value Pr(>|t|)
time1              2.0117     0.7160  178.8300   2.810 0.005510 **
time2             -6.6251     0.6878  160.4000  -9.633  < 2e-16 ***
time3             -3.5668     0.8638  170.9426  -4.129 5.68e-05 ***
time4             -2.4147     0.6889  168.2746  -3.505 0.000584 ***
time1:prepPed     -0.1636     0.3825 4243.7767  -0.428 0.668979
time2:prepPed      1.0020     0.3454 4245.4651   2.901 0.003738 **
time3:prepPed      1.6896     0.4452 4245.5807   3.795 0.000150 ***
time4:prepPed     -0.1672     0.3639 4249.5237  -0.459 0.645996
time1:prepOther    0.1480     0.3270 4224.4539   0.453 0.650877
time2:prepOther    1.9289     0.2847 4220.6930   6.775 1.42e-11 ***
```

```
time3:prepOther    1.1967     0.3678 4222.7422   3.254 0.001146 **
time4:prepOther    1.2110     0.3048 4227.3303   3.973 7.22e-05 ***
```

Table A17a. Model with Coded Interaction Between the Time of the Measurement and the Surgical Technique Variable; forward difference coding, Pedicled Group as Reference

```
summary (x5 <- lmer (green ~ diff.time * prep + (1 | id / time), data))
Linear mixed model fit by REML. t-tests use Satterthwaite's method
['lmerModLmerTest']
Formula: green ~ diff.time * prep + (1 | id/time)
   Data: data

REML criterion at convergence: 21738.7

Scaled residuals:
    Min      1Q  Median      3Q     Max
-6.3801 -0.4604  0.0732  0.5741  4.0383

Random effects:
 Groups   Name        Variance Std.Dev.
 time:id  (Intercept) 11.921   3.453
 id       (Intercept)  3.305   1.818
 Residual              8.285   2.878
Number of obs: 4284, groups:  time:id, 134; id, 46

Fixed effects:
                      Estimate Std. Error        df t value Pr(>|t|)
(Intercept)            -2.0585     0.4237   44.1135  -4.859 1.53e-05 ***
diff.time2-1           -7.4713     0.8557  103.9024  -8.731 4.57e-14 ***
diff.time3-2            3.7459     0.9814  109.3811   3.817 0.000224 ***
diff.time4-3           -0.7047     0.9753  108.9693  -0.723 0.471531
prepSkel               -0.5902     0.1937 4183.4284  -3.047 0.002324 **
prepOther               0.5310     0.1076 4166.5390   4.936 8.27e-07 ***
diff.time2-1:prepSkel  -1.1655     0.5148 4235.9076  -2.264 0.023630 *
diff.time3-2:prepSkel  -0.6876     0.5630 4238.2884  -1.221 0.222009
diff.time4-3:prepSkel   1.8567     0.5744 4235.8645   3.232 0.001237 **
diff.time2-1:prepOther  0.6154     0.2820 4183.8770   2.182 0.029133 *
diff.time3-2:prepOther -1.4198     0.3220 4187.5438  -4.409 1.06e-05 ***
diff.time4-3:prepOther  1.8710     0.3242 4187.8756   5.771 8.45e-09
```

Table A17b. Model with Coded Interaction Between the Time of the Measurement and the Surgical Technique Variable; forward difference coding, reference is the Skeletonised Group

```
summary (x5 <- lmer (green ~ diff.time * prep + (1 | id / time), data))
Linear mixed model fit by REML. t-tests use Satterthwaite's method
['lmerModLmerTest']
Formula: green ~ diff.time * prep + (1 | id/time)
   Data: data

REML criterion at convergence: 21738.7

Scaled residuals:
```

```
    Min      1Q  Median      3Q     Max
-6.3801 -0.4604  0.0732  0.5741  4.0383

Random effects:
 Groups   Name        Variance Std.Dev.
 time:id  (Intercept) 11.921   3.453
 id       (Intercept)  3.305   1.818
 Residual              8.285   2.878
Number of obs: 4284, groups:  time:id, 134; id, 46

Fixed effects:
                       Estimate Std. Error         df t value Pr(>|t|)
(Intercept)            -2.64873    0.44038   51.17798  -6.015 1.92e-07 ***
diff.time2-1           -8.63679    0.91741  136.96101  -9.414  < 2e-16 ***
diff.time3-2            3.05834    1.03325  133.98318   2.960  0.00364 **
diff.time4-3            1.15202    1.03207  134.92710   1.116  0.26631
prepPed                 0.59020    0.19368 4183.42835   3.047  0.00232 **
prepOther               1.12115    0.16164 4182.21806   6.936 4.66e-12 ***
diff.time2-1:prepPed    1.16552    0.51482 4235.90762   2.264  0.02363 *
diff.time3-2:prepPed    0.68760    0.56297 4238.28842   1.221  0.22201
diff.time4-3:prepPed   -1.85671    0.57439 4235.86454  -3.232  0.00124 **
diff.time2-1:prepOther  1.78090    0.43327 4222.43176   4.110 4.03e-05 ***
diff.time3-2:prepOther -0.73217    0.46481 4222.14419  -1.575  0.11529
diff.time4-3:prepOther  0.01425    0.47730 4223.41519   0.030  0.97619
```

10. ACKNOWLEDGEMENTS

I would like to express my deep gratitude to my tutor, Prof. Dr. med. habil. Klaus Matschke, director of the Clinic of Heart Surgery at the Herzzentrum Dresden University Hospital, for endorsing this project and for creating a productive atmosphere that has enabled, and will no doubt continue to enable, the creation of many an inspiring work.

My special thanks go to Dr. med. Stefan Rasche, a consultant doctor at the Clinic of Visceral, Thorax- and Vessel Surgery, an excellent physician and a passionate scientist, whose insights and detailed knowledge of the topic as well as his experience in big data processing in R were invaluable.

The assistance provided by Prof. Dr.-Ing. Sebastian Zaunseder, from the Faculty of Information Technology at the University of Applied Sciences and Arts Dortmund, in the processing of the data was greatly appreciated.

I would like to thank Antje Rost, for her help during the data collection and while working with the patients.

My warmest thanks go to all members of the Intensive Care Unit in the Clinic of Heart Surgery of the Herzzentrum Dresden University Hospital for allowing the seamless realisation of the measurements as well as for their support during my time in the clinic.

Last but not least, I want to thank my wife, Dr. Flóra Hajdu, for her unwavering support and advice during the creation of this work.

11. RESUME

Due to data protection concerns the electronic version of the dissertation does not contain my resume.

Anlage 1

Technische Universität Dresden
Medizinische Fakultät Carl Gustav Carus
Promotionsordnung vom 24. Juli 2011

Erklärungen zur Eröffnung des Promotionsverfahrens

1. Hiermit versichere ich, dass ich die vorliegende Arbeit ohne unzulässige Hilfe Dritter und ohne Benutzung anderer als der angegebenen Hilfsmittel angefertigt habe; die aus fremden Quellen direkt oder indirekt übernommenen Gedanken sind als solche kenntlich gemacht.

2. Bei der Auswahl und Auswertung des Materials sowie bei der Herstellung des Manuskripts habe ich Unterstützungsleistungen von folgenden Personen erhalten:

Dr. med. Stefan Rasche

3. Weitere Personen waren an der geistigen Herstellung der vorliegenden Arbeit nicht beteiligt. Insbesondere habe ich nicht die Hilfe eines kommerziellen Promotionsberaters in Anspruch genommen. Dritte haben von mir weder unmittelbar noch mittelbar geldwerte Leistungen für Arbeiten erhalten, die im Zusammenhang mit dem Inhalt der vorgelegten Dissertation stehen.

4. Die Arbeit wurde bisher weder im Inland noch im Ausland in gleicher oder ähnlicher Form einer anderen Prüfungsbehörde vorgelegt.

5. Die Inhalte dieser Dissertation wurden in folgender Form veröffentlicht:

Kukel, I., Trumpp, A., Plötze, K., Rost, A., Zaunseder, S., Matschke, K., & Rasche, S. (2020). Contact-Free Optical Assessment of Changes in the Chest Wall Perfusion after Coronary Artery Bypass Grafting by Imaging Photoplethysmography. *Applied Sciences, 10*(18), 6537. https://doi.org/10.3390/app10186537

6. Ich bestätige, dass es keine zurückliegenden erfolglosen Promotionsverfahren gab.

7. Ich bestätige, dass ich die Promotionsordnung der Medizinischen Fakultät der Technischen Universität Dresden anerkenne.

8. Ich habe die Zitierrichtlinien für Dissertationen an der Medizinischen Fakultät der Technischen Universität Dresden zur Kenntnis genommen und befolgt.

Dresden, den 30.11.2021

Unterschrift des Doktoranden

Anlage 2

Hiermit bestätige ich die Einhaltung der folgenden aktuellen gesetzlichen Vorgaben im Rahmen meiner Dissertation

- ☐ das zustimmende Votum der Ethikkommission bei Klinischen Studien, epidemiologischen Untersuchungen mit Personenbezug oder Sachverhalten, die das Medizinproduktegesetz betreffen
  Aktenzeichen der zuständigen Ethikkommission

  IRB00001473, EK168052013

- ☐ die Einhaltung der Bestimmungen des Tierschutzgesetzes
  Aktenzeichen der Genehmigungsbehörde zum Vorhaben/zur Mitwirkung:

  trifft nicht zu.

- ☐ die Einhaltung des Gentechnikgesetzes

  Projektnummer: trifft nicht zu.

- ☐ die Einhaltung von Datenschutzbestimmungen der Medizinischen Fakultät und des Universitätsklinikums Carl Gustav Carus.

Dresden, den 30.11.2021

Unterschrift des Doktoranden